

Large eddy simulations of turbulent planar jets of viscoelastic fluids

Cite as: Phys. Fluids **33**, 000000 (2021); doi: [10.1063/5.0039826](https://doi.org/10.1063/5.0039826)

Submitted: 7 December 2020 · Accepted: 15 February 2021 ·

Published Online: 0 Month 0000



S. Parvar,^{1,2} C. B. da Silva,³ and F. T. Pinho^{1,a)}

AFFILIATIONS

¹CEFT/FEUP, Universidade do Porto, Rua Dr. Roberto Frias, 4200-465 Porto, Portugal

²INEGI, Campus da FEUP, Rua Dr. Roberto Frias, 4200-465 Porto, Portugal

³LAETA, IDMEC, Instituto Superior Técnico, Universidade de Lisboa, Lisboa, Portugal

^{a)}Author to whom correspondence should be addressed: fpinho@fe.up.pt

ABSTRACT

Direct numerical simulations and large-eddy simulations of turbulent planar jets are used to assess the distortion similarity (DSIM) model, recently developed by Ferreira *et al.* [“Large-eddy simulations of forced isotropic turbulence with viscoelastic fluids described by the finitely extensible nonlinear elastic rheological model with Peterlin’s closure model,” Phys. Fluids **28**, 125104 (2016)] for homogeneous turbulence, in the simulation of turbulent viscoelastic planar jets. Both *a priori* and *a posteriori* tests of the DSIM model are used and show that the several assumptions used in the development of the DSIM model hold well in inhomogeneous free turbulent viscoelastic flows, e.g., (i) the scale similarity of the subgrid-scale (SGS) polymer stretching and (ii) the local equilibrium of the elastic energy production and dissipation. The DSIM model for the SGS polymer stretching term, together with the dynamic Smagorinsky model, is able to reproduce well the flow structures and the classical one-point statistics of turbulent viscoelastic planar jets. The model should be equally able to simulate other free shear flows of viscoelastic fluids, e.g., wakes and mixing layers.

Published under license by AIP Publishing. <https://doi.org/10.1063/5.0039826>

NOMENCLATURE

A_{U_c}	The slope of the law of variation of centerline velocity (–)
A_δ	The slope of the law of variation of the jet width (–)
A_{τ_c}	The slope of the laws of variation of centerline stress (–)
C_{Dyn}	Coefficient of dynamic Smagorinsky model (–)
C_{ij}	Conformation tensor (–)
C_{sm}	Coefficient of classical Smagorinsky model (–)
$E(\kappa)$	Energy spectrum ($\text{m}^2 \text{s}^2$)
$f(C_{kk})$	Peterlin function (–)
H	Width of the inlet slot (m)
L	Dumbbell maximum extensibility (–)
L_x, L_y, L_z	Computational domain length in the x, y, z directions (m)
n_x, n_y, n_z	Number of grid points in the x, y, z directions
P	Pressure (Pa)
Re	Reynolds number (–)
S_{ij}	Strain rate tensor (s^{-1})
$ S $	Norm of the strain rate tensor (s^{-1})

T	Time (s)	45
u, v, w	Velocity in streamwise, normal, and spanwise direction (ms^{-1})	46
u_i	Velocity vector (ms^{-1})	47
U_j	Peak velocity at the inlet (ms^{-1})	48
U_∞^{in}	Co-flow velocity (ms^{-1})	49
x_i	<i>i</i> -th space coordinate (m)	50
X'	Fluctuation of X	51
\bar{X}	X low pass filtered in space	52
$\langle X \rangle_a$	Spatial averaging of X along <i>a</i> -direction	53

Greek letter

β	Ratio of kinematic viscosities (–)	54
δ_{ij}	Kronecker delta	55
δ_u	Mean flow thickness of the planar jet (m)	56
Δ	Filter size (m)	57
Δt	Time step (m)	58
$\Delta x, \Delta y, \Delta z$	Grid spacing in the x, y, z directions (m)	59
ε_s	Turbulent kinetic energy dissipation ($\text{m}^2 \text{s}^{-3}$)	60
η	Kolmogorov length micro-scale (m)	61

66	κ	Wave number (m^{-1})
67	λ	Relaxation time of polymer (s)
68	ν_p	Polymer kinematic viscosity ($\text{m}^2 \text{s}^{-1}$)
69	ν_s	Solvent kinematic viscosity ($\text{m}^2 \text{s}^{-1}$)
70	ν_t	Turbulent kinematic viscosity ($\text{m}^2 \text{s}^{-1}$)
71	ρ	Fluid density (kg m^{-3})
72	τ_{ij}^p	Polymer stress tensor (Pa)
73	τ_{ij}^r	Residual stress tensor (Pa)
74	τ_{ij}^s	Solvent stress tensor (Pa)
75	ψ_{ij}	SGS polymer convection tensor (s^{-1})
76	ω	Vorticity vector (s^{-1})

79 Subscripts and superscripts

80	[s]	Refers to solvent
81	[p]	Refers to polymer

83 I. INTRODUCTION

84 In 1949, Toms¹ found that adding a small number of polymeric
 85 molecules into Newtonian fluids induces severe drag reduction (DR), of
 86 up to 80% in turbulent pipe flow, which also naturally leads to a concomi-
 87 tant reduction in heat transfer. Industrial settings where viscoelastic fluids
 88 flow under turbulent conditions and lead to DR are oil transport in
 89 pipelines and well drilling for the oil and gas industries.² Other proposals
 90 have been put forward to use viscoelastic fluids in order to benefit from
 91 turbulent drag and heat transfer reductions such as in district heating
 92 and cooling systems,³ firefighting equipment, and sewage systems.
 93 Operation in these two last applications are under extreme conditions: in
 94 firefighting, the aim is to increase the length of the jet, whereas the
 95 increase in flow rate at constant head due to drag reduction is very useful
 96 to increase the capacity of sewage systems during floods.⁴ Other fields of
 97 application include the design of ships and submarines since drag reduction
 98 leads to more efficient energy use,⁵ increasing the mixing rates in
 99 microfluidic applications⁶ and biofluid systems.^{7,8} Reducing the energy
 100 consumption rate in irrigation systems and in percolation through the
 101 soil is another motivation to use this phenomenon.⁹ Some applications of
 102 drag reduction with viscoelastic fluids are also encountered in medicine
 103 during surgery when some blood analogs are used.^{10,11} Hence, it comes
 104 as no surprise that the wealth of research on this topic was reviewed in
 105 detail by Lumley,¹² Virk¹³ and more recently White and Mungal.¹⁴

106 Direct numerical simulation (DNS) is the most accurate existing
 107 numerical technique to simulate turbulent flows. However, it requires
 108 very fine computational grids, with the number of grid points on the
 109 order of $O(Re^{9/4})$, and very small time steps in order to capture all the
 110 multiscale features of turbulent motion,^{15,16} in addition to large mem-
 111 ory requirements. For these reasons, DNS is not suited for fast engi-
 112 neering calculations and is still restricted to simple flows at moderate
 113 Reynolds numbers for assisting our understanding of the flow physics
 114 and the development of turbulence models for engineering computa-
 115 tions.¹⁷ This is particularly true when one considers DNS of turbulent
 116 flows of viscoelastic fluids since the computational cost of these simula-
 117 tions is substantially higher than for DNS of Newtonian fluids due to
 118 the additional rheological variables and corresponding governing equa-
 119 tions and the numerical limitations imposed by fluid viscoelasticity.

120 Currently, the numerical simulation of engineering flows under
 121 turbulent flow conditions relies on the use of the Reynolds-averaged

Navier–Stokes equations (RANS) proposed by Reynolds¹⁸ due to the
 low or reasonable computational cost. RANS is based on the Reynolds
 decomposition of the physical variables and subsequent averaging of
 the governing equations, which introduces new unknowns that need
 to be modeled. There are some available RANS models for turbulent
 flows of viscoelastic fluids,^{19–23} which were developed based on wall
 turbulent flows. However, RANS has well known limitations when
 dealing with unsteady and transient flows, flows with separation, and
 rotation and flows faced with strong curvatures. Moreover, although
 RANS models may be able to predict the mean properties of the many
 flows, many important characteristics of the flow cannot be estimated,
 such as the dominating flow frequencies. Large eddy simulation (LES)
 is a numerical technique that is usually suggested as the best candidate
 to handle the limitations of RANS without incurring in the massive
 cost of DNS. LES can be seen as an intermediate approach between
 DNS and RANS, which was initially developed to simulate atmo-
 spheric flows²⁴ and that was latter used to simulate wall bounded
 flows.²⁵ In LES, the large scales of motion (or resolved or grid-scales,
 GS) are explicitly simulated, while the effects of the small scales of
 motion, or subgrid-scales (SGS), are modeled. The SGS term arises
 when low-pass filtering the Navier–Stokes equations and needs to be
 modeled. A comprehensive review of LES approaches can be found in
 Refs. 26–28.

The main role of any SGS model consists in assuring the correct
 amount of kinetic energy transfer between the resolved and unresolved
 scales, and is consequently heavily derived from the classical
 Richardson–Kolmogorov energy cascade concept.^{15,29} When the turbu-
 lence arises in a non-Newtonian fluid, the energy cascade mechanism
 becomes considerably more complicated due to the interaction of the
 velocity fluctuations with the fluid rheology variables across a large
 range of space and time scales. Indeed, non-Newtonian fluids are char-
 acterized by a variety of rheological constitutive equations.^{30,31} There
 are ongoing debates regarding what are the appropriate constitutive
 equations needed to describe dilute polymer solutions.^{32,33} However,
 one of the simplest constitutive equations used is the finitely extensible
 nonlinear elastic rheological model with Peterlin’s closure (FENE-P),
 which is able to describe the main features of the rheology of dilute
 polymer solutions,^{30,31,34–36} such as memory effects, shear-thinning,
 and bounded elastic stresses. For these reasons, the FENE-P model has
 been used in many studies of turbulent viscoelastic fluid flows.^{37–40}

The interaction between the solvent and the polymer molecules
 greatly complicates the kinetic energy cascade, particularly in the
 so-called inertio-elastic turbulence, which occurs when the polymer
 relaxation times are larger than the Kolmogorov time scale.^{37,40} For
 instance, it was observed that in this regime the polymer additives dis-
 sipate the main portion of the kinetic energy transferred from the large
 to the small scales of motion, which may lead to the establishment of a
 second, polymer induced, kinetic energy cascade.^{37–40} This polymer-
 induced energy cascade competes with the classical (nonlinear) energy
 cascade^{39–41} and therefore greatly complicates the GS/SGS interactions
 that play a vital role in the dynamics of turbulent flows and that need
 to be understood and modeled into the SGS terms aiming to simulate
 turbulence in viscoelastic fluids. Note in this respect that low-pass
 filtering the rheological constitutive equation for viscoelastic fluids also
 gives rise to new SGS terms there.

There are only a few studies about the SGS model in the momen-
 tum equation for turbulent flows of non-Newtonian fluids. Ohta and

Miyashita⁴² extended the Smagorinsky model, by considering the effect of variable viscosity, to study turbulent channel flow of various types of purely viscous non-Newtonian fluids based on power laws. Thais *et al.*⁴³ proposed the first SGS model for temporal large eddy simulations (TLES) of viscoelastic fluid flows based on the FENE-P constitutive equation. Their SGS model was based on a temporal approximate deconvolution method (TADM) for both the SGS terms of the solvent and polymer stresses in momentum and conformation tensor equations. Although the TLES model has good accuracy in DR predictions, at least when using fine meshes, it is highly complex because of the deconvolution procedures involved, and for this reason, it is likely to demand considerable computational cost. Moreover, the model is entirely based on mathematical procedures, without any physical input from the interaction between the turbulent fluctuations and the fluid elasticity. Wang *et al.*⁴⁴ used the TLES model in forced homogeneous isotropic turbulence (FHIT) of FENE-P fluids at moderate Taylor scale Reynolds number and verified the results with the corresponding DNS results. Li *et al.*⁴⁵ investigated the DR in viscoelastic turbulent channel flows using the TLES model⁴³ by filtering their constitutive equation, a simplified version of a multi-mode FENE-P model.

Masoudian *et al.*⁴⁶ carried out *a priori* tests in order to analyze and evaluate the effect of the polymer additives on the SGS energy in the filtered momentum and FENE-P constitutive equations in turbulent channel flow of viscoelastic fluids. They were able to identify which terms become negligible and which require modeling when the filtering operation was applied to the FENE-P evolution equations. The subgrid-scale advection term in the filtered conformation tensor equation is an example of the former, whereas the subgrid-scale distortion in the same equation is an example of the latter.

To deal with the subgrid-scale distortion in the evolution equation for the conformation tensor in LES of forced isotropic turbulence of viscoelastic fluids, described by the FENE-P model, Ferreira *et al.*³⁷ proposed the distortion similarity model (DSIM). The SGS stresses arising in the solvent were modeled with the classical Smagorinsky model. The DSIM model relies on two main assumptions: (i) self-similarity of the polymer stretching term and (ii) global/local equilibrium of the trace of conformation tensor. The LES results from the DSIM model show that it predicts well many detailed quantities from forced isotropic turbulence of viscoelastic fluids, such as the solvent dissipation reduction (SDR), the shape of the kinetic energy spectra, and the shape and size of the coherent vortices. It is noteworthy that in contrast to previous models the DSIM model is simple to implement and exhibits a low computational cost.

The main motivation of the present work is to assess the DSIM model recently developed by Ferreira *et al.*³⁷ in inhomogeneous turbulent flow configurations. This model has been previously developed and assessed in isotropic turbulence, and it is important to test its performance in flows characterized by inhomogeneous conditions in order to isolate these conditions in the results obtained from the model. Although the ultimate goal of any newly developed subgrid-scale model must be to accurately simulate wall bounded flows, it is also well known that LES of wall bounded flows faces considerable challenges that have not much to do with the core of the subgrid-scale model,¹⁵ and the analysis of new subgrid-scale models is often blurred when they are assessed initially in wall flows due to the restricted “activity” of the models near walls.

Consequently, in the present study, we assess the DSIM model in a planar turbulent jet flow since it provides a simple configuration to consider the effects of inhomogeneity, without facing the difficulties that arise in the presence of solid walls. Our study is inspired from Masoudian *et al.*⁴⁶ and uses the recently published DNS results from Guimarães *et al.*⁴⁷ to assess several modeling hypotheses. Then, the DSIM subgrid-scale model is implemented in our in-house DNS code and its performance is assessed through *a posteriori* tests.

The paper is organized as follows. Sections II and III discuss the flow problem and present the governing equations for flows of viscoelastic fluids described by FENE-P model and filtered governing equations, respectively. Section IV presents the main numerical techniques and algorithms used in the present study. Sections V and VI assess the model using *a priori* and *a posteriori* tests, respectively. The paper ends with an overview of the main conclusions.

II. FLOW PROBLEM AND GOVERNING EQUATIONS

A planar jet is a type of free shear layer flow in which a stream of high momentum is discharged into the same or another fluid at rest; in this work, the former situation is considered. Figure 1 shows the Cartesian coordinate system used in the present work, where the main flow direction (streamwise) is x , and the jet spreads in the normal direction (y), while the flow is homogeneous in the spanwise (z) direction. U_j is the uniform streamwise velocity at the inlet nozzle, U_∞ is the jet co-flow velocity, and H is the inlet slot-width of the jet. According to the classical jet theory (for a Newtonian fluid), the turbulent planar jet flow in the far field is statistically two-dimensional and is independent of Reynolds number, provided the Reynolds number is high enough.¹⁵

The jet half-width is defined as the transverse distance between the centerline and the location where the mean streamwise velocity equals half the mean centerline velocity; however, in the present study, we use a different definition for the jet shear layer thickness $\delta(x)$, introduced by Guimarães *et al.*⁴⁷ It assumes that the volumetric flow rate remains constant and is equal to $\dot{V}(x) = 2L_z\delta(x)U_c(x)$, where $U_c(x)$ is the value of the mean velocity at the centerline and L_z is the computational domain length in the spanwise direction. Since the flow

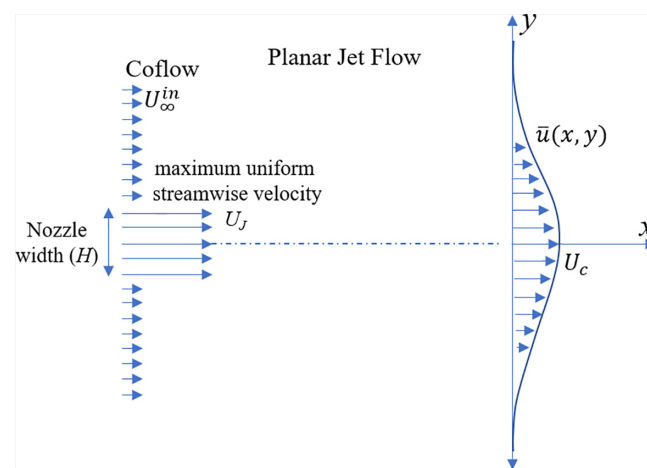


FIG. 1. The schematic of planar jet flow.

272 rate of the jet is obtained from $\dot{V}(x) = 2L_z \int_0^\infty \bar{u}(x, y) dy$, the jet shear
 273 thickness defined in Ref. 47 is

$$\delta(x) = \int_0^\infty \frac{\bar{u}(x, y)}{U_c(x)} dy, \quad (1)$$

274 where $\bar{u}(x, y)$ is the profile of mean streamwise velocity.

275 **A. The governing equations of FENE-P fluids**

276 The FENE-P model is used to describe the rheology of the dilute
 277 polymer solutions. In this model, the effects of an ensemble of mole-
 278 cules located at any given point are represented by dumbbells, each
 279 consisting of a pair of beads connected by a massless nonlinear spring.

280 The mass conservation and momentum equations for an incom-
 281 pressible isothermal flow are

$$\frac{\partial u_k}{\partial x_k} = 0, \quad (2)$$

$$\rho \left(\frac{\partial u_i}{\partial t} + u_k \frac{\partial u_i}{\partial x_k} \right) = - \frac{\partial P}{\partial x_i} + \frac{\partial \tau_{ij}}{\partial x_k}, \quad (3)$$

282 where u_i is the velocity vector, P is the pressure, ρ is the fluid density,
 283 and τ_{ij} is the total stress tensor which is calculated as the sum of a
 284 Newtonian solvent contribution (τ_{ij}^s) and a polymeric contribution
 285 (τ_{ij}^p)^{19,20,30,31}

$$\tau_{ij} = \tau_{ij}^s + \tau_{ij}^p. \quad (4)$$

286 The solvent stress τ_{ij}^s is described by Newton's law of viscosity with sol-
 287 vent kinematic viscosity ν_s

$$\tau_{ij}^s = 2\rho\nu_s S_{ij}, \quad (5)$$

288 where S_{ij} is the rate-of-strain tensor, defined as

$$S_{ij} = \frac{1}{2} \left(\frac{\partial u_i}{\partial x_j} + \frac{\partial u_j}{\partial x_i} \right). \quad (6)$$

289 The polymeric stress (τ_{ij}^p) of the FENE-P model relies on the following
 290 explicit equation:^{19,20,30,31}

$$\tau_{ij}^p = \frac{\rho\nu_p}{\lambda} [f(C_{kk})C_{ij} - f(L)\delta_{ij}], \quad (7)$$

291 where ν_p is the polymer zero shear rate kinematic viscosity and C_{ij} is
 292 the conformation tensor. The conformation tensor expresses the ori-
 293 entation and stretch of the set of polymer dumbbells at each point,
 294 which is defined as

$$C_{ij} = \frac{\langle r_i r_j \rangle}{\langle R^2 \rangle_0}, \quad (8)$$

295 where r_i is the end-to-end projection in i -direction of the vector con-
 296 necting the two beads of the dumbbell. The second order moment
 297 $\langle r_i r_j \rangle$ is normalized by the square of its equilibrium radius $\langle R^2 \rangle_0$,
 298 where $\langle \rangle$ represents an ensemble average over the configuration
 299 space of the dumbbells. The FENE-P model also depends on λ , which
 300 is the longest relaxation time of the polymer molecules and δ_{ij} is the
 301 identity tensor. The Peterlin function is expressed by

$$f(C_{kk}) = \frac{L^2 - 3}{L^2 - C_{kk}}, \quad (9)$$

and its value at equilibrium is $f(L) = 1$, where L is the maximum
 dumbbell extensibility and C_{kk} is the trace of the conformation tensor.
 The conformation tensor obeys the following hyperbolic differential
 equation:

$$\frac{\partial C_{ij}}{\partial t} + u_k \frac{\partial C_{ij}}{\partial x_k} = C_{jk} \frac{\partial u_i}{\partial x_k} + C_{ik} \frac{\partial u_j}{\partial x_k} - \frac{1}{\lambda} [f(C_{kk})C_{ij} - f(L)\delta_{ij}]. \quad (10)$$

The first term on the left-hand side (LHS) of Eq. (10) is the local time
 variation of conformation tensor and the second term is the advection
 term, while the first two terms on the right-hand side (RHS) account
 for the stretching and distortion of the polymer molecules. The last
 term on RHS represents the storage of elastic energy in the polymer
 molecules.

The two kinematic viscosity coefficients defined the solvent vis-
 cosity ratio $\beta_s = \frac{\nu_s}{\nu_s + \nu_p} = \frac{\nu_s}{\nu_0}$, where the zero-shear rate viscosity of the
 fluid (ν_0) is the sum of solvent and polymer kinematic viscosities
 $\nu_0 = \nu_s + \nu_p$. Since the FENE-P model is used to describe dilute poly-
 mer solutions, the value of β_s in this work is restricted to
 $0.8 \leq \beta_s \leq 1$.

The governing equations above are valid for DNS of a viscoelastic
 flow described by the FENE-P model. However, the governing equa-
 tions required for LES involve several additional SGS terms as
 described in Sec. III.

322 **III. FILTERED GOVERNING EQUATIONS**

To obtain the governing equation for LES of the viscoelastic flu-
 ids described by the FENE-P model, one needs to filter the equations
 of Sec. II, as described in detail in Masoudian *et al.*⁴⁶ and in Ferreira
et al.,³⁷ so that any flow variable $\varphi(\vec{x}, t)$, is split into the sum of a
 resolved (grid-scale-GS) $\overline{\varphi}(\vec{x}, t)$, and an unresolved (subgrid-scale-
 SGS), contribution

$$\varphi(\vec{x}, t) = \overline{\varphi}(\vec{x}, t) + \varphi'(\vec{x}, t). \quad (11)$$

The GS contribution is defined by a spatial low pass filtering operation

$$\overline{\varphi}(\vec{x}, t) = \int_{\Omega} \overline{\varphi}(\vec{x}', t) G_{\Delta}(\vec{x} - \vec{x}') d\vec{x}', \quad (12)$$

in which G_{Δ} is the convolution kernel that determines the filter type,
 and Δ is the filter width. In the present study, a classical top-hat (box)
 convolution filter is utilized to separate the resolved and unresolved
 scales of motion, which for a one-dimensional case reads as

$$G_{\Delta}(x) = \begin{cases} \frac{1}{\Delta} & \text{if } |x| \leq \frac{\Delta}{2} \\ 0 & \text{otherwise} \end{cases}. \quad (13)$$

The box filter is local in the physical space and nonlocal in the spectral
 space, but the filtering operation is equivalent to a finite difference or
 finite volume discretization, which are commonly used in LES of engi-
 neering applications.¹⁶ By applying the low pass filter to the governing
 equations, the filtered continuity and momentum equations are
 obtained (Masoudian *et al.*⁴⁶ and in Ferreira *et al.*³⁷)

$$\frac{\partial \bar{u}_k}{\partial x_k} = 0, \tag{14}$$

$$\frac{\partial \bar{u}_i}{\partial t} + \bar{u}_k \frac{\partial \bar{u}_i}{\partial x_k} = -\frac{1}{\rho} \frac{\partial \bar{P}}{\partial x_i} + \nu_s \frac{\partial}{\partial x_k} [2\bar{S}_{ij}] + \frac{\partial \tau_{ij}^{SGS}}{\partial x_k} + \frac{\partial \bar{\tau}_{ij}^p}{\partial x_k}, \tag{15}$$

where $\tau_{ij}^{SGS} = [\bar{u}_i \bar{u}_j - \bar{u}_i \bar{u}_j]$ is the SGS tensor and the last term on the RHS of Eq. (15) is the filtered polymer stress contribution given by

$$\bar{\tau}_{ij}^p = \frac{\rho \nu_p}{\lambda} \left[\overline{f(C_{kk}) C_{ij}} - f(L) \delta_{ij} \right]. \tag{16}$$

Equation (16) can be re-written as

$$\bar{\tau}_{ij}^p = \frac{\rho \nu_p}{\lambda} \left[f(\bar{C}_{kk}) \bar{C}_{ij} + \chi_{ij} - f(L) \delta_{ij} \right]. \tag{17}$$

in which the SGS of the filtered $\overline{f(C_{kk}) C_{ij}}$, is defined as

$$\chi_{ij} = \overline{f(C_{kk}) C_{ij}} - f(\bar{C}_{kk}) \bar{C}_{ij}. \tag{18}$$

The filtered evolution equation for the conformation tensor is

$$\frac{\partial \bar{C}_{ij}}{\partial t} + u_k \frac{\partial \bar{C}_{ij}}{\partial x_k} = \frac{\partial \bar{u}_i}{\partial x_k} \bar{C}_{jk} + \frac{\partial \bar{u}_j}{\partial x_k} \bar{C}_{ik} - \frac{1}{\lambda} \left[\overline{f(C_{kk}) C_{ij}} - \delta_{ij} \right], \tag{19}$$

where the last term on the LHS is the filtered advection of the conformation tensor, and the first two terms on the RHS are the filtered polymer stretching, whereas the last term on the RHS is the filtered polymer dissipation. Equation (19) can be re-written in a way that singles out the resolved and subgrid-scale quantities in the conformation tensor equation as discussed previously,^{37,46} namely,

$$\frac{\partial \bar{C}_{ij}}{\partial t} + \bar{u}_k \frac{\partial \bar{C}_{ij}}{\partial x_k} = \frac{\partial \bar{u}_i}{\partial x_k} \bar{C}_{jk} + \frac{\partial \bar{u}_j}{\partial x_k} \bar{C}_{ik} - \frac{1}{\lambda} \left[f(\bar{C}_{kk}) \bar{C}_{ij} + \chi_{ij} - \delta_{ij} \right] - \psi_{ij} + \gamma_{ij}, \tag{20}$$

with χ_{ij} defined in Eq. (18), the unresolved (SGS) conformation advection tensor defined as

$$\psi_{ij} = u_k \frac{\partial \bar{C}_{ij}}{\partial x_k} - \bar{u}_k \frac{\partial \bar{C}_{ij}}{\partial x_k}, \tag{21}$$

and the SGS polymer stretching tensor given by

$$\gamma_{ij} = \left[\frac{\partial \bar{u}_i}{\partial x_k} \bar{C}_{jk} - \frac{\partial \bar{u}_i}{\partial x_k} \bar{C}_{jk} \right] + \left[\frac{\partial \bar{u}_j}{\partial x_k} \bar{C}_{ik} - \frac{\partial \bar{u}_j}{\partial x_k} \bar{C}_{ik} \right]. \tag{22}$$

Now, closures need to be developed for all SGS terms in all governing equations. In principle the SGS stress tensor in the momentum equation may be affected by fluid rheology. However, since this is the very first work developing models for LES of viscoelastic fluids in jets and τ_{ij}^{SGS} quantifies inertial effects, as a first approximation we will consider that the closures developed for τ_{ij}^{SGS} with Newtonian fluids remain valid and the effect of polymers on it is carried over through the filtered velocity and rate of deformation fields. The closures used for τ_{ij}^{SGS} are presented next.

A. Smagorinsky model (Sm)

Solution of the LES equations requires closures for all the SGS terms. In the present work the SGS stress tensor τ_{ij}^{SGS} is modeled using

two different closures: the classical and the dynamic Smagorinsky models. Both models were previously implemented in the present planar jet flow code (for Newtonian fluids) by Silva *et al.*^{48,49}

The Smagorinsky model was originally developed by Smagorinsky⁵⁰ and is based on an eddy viscosity given by

$$\nu_t(x, t) = (C_{Sm} \bar{\Delta})^2 |\bar{S}|, \tag{23}$$

where $|\bar{S}| = (2\bar{S}_{ij}\bar{S}_{ij})^{1/2}$ is the filtered strain magnitude, and \bar{S}_{ij} is the filtered rate-of-strain which is obtained by filtering Eq. (6), C_{Sm} is the Smagorinsky constant, and $\bar{\Delta}$ is the filter size calculated by $\bar{\Delta} = (\Delta x \times \Delta y \times \Delta z)^{1/3}$.¹⁶ The main drawback of the classical Smagorinsky model is that it cannot consider backward energy transfer since it is a dissipative closure: the local equilibrium assumption is not valid and the model is too dissipative. However, the Smagorinsky model is simple, with a very low computational cost; therefore, it is popular in the study of turbulent flows. In the present work, we take $C_{Sm} = 0.16$ for the Smagorinsky constant.^{48,49} This model, with the same value of C_{Sm} , was used previously by Ferreira *et al.*³⁷ for FENE-P fluids in forced homogeneous isotropic turbulence, with very good results.

B. Dynamic Smagorinsky model (Dyn)

To deal with the limitations of the classical Smagorinsky closure, the dynamic Smagorinsky model was proposed by Germano *et al.*⁵¹ Here, the eddy viscosity is still given by Eq. (23), but with C_{Dyn} instead of C_{Sm} , where C_{Dyn} is assumed to depend on time and space and computed by utilizing the Germano identity. As a result, the coefficient is now computed in the entire domain as $C_{Dyn}(x, y, t) = \frac{\langle M_{ij} L_{ij} \rangle}{\langle M_{ij} M_{ij} \rangle}$, where $\langle \rangle$ represents an averaging in the homogenous flow direction, which in the present planar jet flow is the z -direction. The coefficient depends on the Leonard stress tensor

$$L_{ij} = \bar{u}_i \bar{u}_j - \tilde{u}_i \tilde{u}_j, \tag{24}$$

obtained by applying a spatial test filter, of size equal to 2Δ and identified by the tilde, and on

$$M_{ij} = (k\Delta)^2 |\tilde{S}| \tilde{S}_{ij} - \Delta^2 |\bar{S}| \bar{S}_{ij}. \tag{25}$$

For a test filter size equal to 2Δ , the coefficient k is assumed to be $k = \sqrt{5}$, $|\bar{S}|$ is defined in Sec. III B and $|\tilde{S}| = \sqrt{2\tilde{S}_{ij}\tilde{S}_{ij}}$ is the magnitude of the double filter sized of the large-scale strain rate tensor. To prevent the existence of numerical instabilities during the simulations due to excessively large negative values of coefficient C_{Dyn} , a clipping procedure was implemented and $C_{Dyn} \geq 0$ was imposed everywhere.

IV. NUMERICAL METHODS

The in-house code used to solve the original governing equations through DNS and the filtered governing equation (LES) is the same. Recently, our in-house DNS solver has been extended by Guimarães *et al.*⁴⁷ to simulate turbulent flows of FENE-P fluids. The code was originally developed by Reis⁵² and later by Lopes⁴⁸ who added some LES closures^{48,49} for Newtonian fluids. The code uses a sixth-order compact differencing scheme⁵³ in the streamwise (x) direction and a pseudo-spectral method⁵⁴ in the normal (y) and spanwise (z) directions.²⁹ An explicit three-step third-order low-storage Runge-Kutta

time-stepping scheme is used for temporal discretization. For the present studies, the new closures associated with the constitutive equations, to be discussed below, were added to the code.

Discontinuities in the polymer stresses are the main difficulty in implementing the FENE-P model because of the growth of Hadamard instabilities.⁵⁵ Several methods have been proposed by utilizing artificial stress diffusivity or the slope limiter to handle this problem such as.^{56–60} Although they can prevent the Hadamard instabilities, they may affect the computation of the polymer stresses or produce negative eigenvalues in the conformation tensor, leading to errors in the conservation laws.^{58–61} In 2006, Vaithianathan *et al.*⁶¹ utilized the Kurganov and Tadmor (or KT)⁶² numerical scheme to handle all mentioned issues. The KT scheme is a central difference, second-order accurate in physical space, and independent of the time step. The KT scheme assures that the conservation laws for conformation tensor are satisfied. Details of this procedure in the present code are described in detail in Refs. 47, 62, and 63. The implementation of the KT scheme in the present code was carried out by Guimarães *et al.*⁴⁷ and the semi-analytical solution for the laminar planar jet flow of FENE-P fluids of Parvar *et al.*^{64,65} was also used to verify the implementation.

V. A PRIORI TESTS: DNS OF TURBULENT PLANAR JET FENE-P FLUID

To develop closures for the remaining SGS terms, appearing in the constitutive equation, we perform *a priori* tests by using the DNS data of turbulent viscoelastic planar jet flows of Guimarães *et al.*⁴⁷ The physical and computational characteristics of these simulations are now described, with more details given in Guimarães *et al.*⁴⁷

A hyperbolic tangent profile is used as an inlet condition for the mean inlet velocity profile,²⁹

$$\bar{u}(x = 0, y) = \frac{U_j + U_\infty^{\text{in}}}{2} + \frac{U_j - U_\infty^{\text{in}}}{2} \tanh \left[\frac{H}{4\theta} \left(1 - \frac{2|y|}{H} \right) \right], \quad (26)$$

where U_j is the maximum mean streamwise velocity and U_∞^{in} is the jet co-flow velocity, and for the conformation tensor profiles at the inlet, conditions of fully-developed channel flow were assumed with the shear rate computed from the velocity profile of Eq. (26), as given by Pinho *et al.*¹⁹ Periodic boundary conditions are used for the lateral boundaries (y and z directions). In addition, the amplitude of noise for all inlet velocity fluctuations of DNS is set at 10%, and the ratio between the inlet slot-width and the momentum thickness is $H/\theta = 30$.^{47,49} The Reynolds number (Re) is defined by

$$Re_H = \frac{(U_j - U_\infty^{\text{in}})H}{\nu_s}, \quad (27)$$

where H is the inlet slot-width of the jet and ν_s is the kinematic solvent viscosity. A global Weissenberg number is also defined as the ratio between the elastic and integral time scales, which for the turbulent jet is given by

$$Wi = \frac{\lambda(U_j - U_\infty^{\text{in}})}{H}. \quad (28)$$

In all simulations the Reynolds number was equal to $Re = 3500$, and the ratio between the solvent and the total viscosities (β_s) was set to $\beta_s = 0.8$. The computational domain length was equal to $18H$ and the grid size was $512 \times 512 \times 128$ in the streamwise, normal, and spanwise

directions, respectively. The maximum extensibility of the dumbbell was set to $L^2 = 10^4$, while the relaxation time for the FENE-P fluid flows were $\lambda = 0.4, 0.8$ and 1.2 s, leading to the global Weissenberg numbers of $Wi = 1.1, 2.2,$ and $3.3,$ respectively. A reference Newtonian DNS was also carried out for comparison and its results are indicated by subscript N. The main physical and computational details of the DNS are summarized in Table I (data extracted from Guimarães *et al.*⁴⁷).

The statistical data extracted from the DNS of Guimarães *et al.*⁴⁷ was initially used to analyze the order of magnitude of each term in Eqs. (20)–(22), in order to simplify those equations by proposing relevant hypothesis, named (H1)–(H6) and finally to introduce the set of LES closures. It is important to mention that *a priori* tests were performed on the available instantaneous DNS data provided by Guimarães *et al.*,⁴⁷ but since the number of continuous instants of time provided was not very large, if we consider data at a specific x, y location the sample size is limited, even if data are averaged in the homogeneous direction (z), which we always do. Therefore, in order to increase the sample size we decided to perform the tests for the assessment of all hypotheses using the combination of all instantaneous data at the jet centerline ($y/H = 0$) inside the self-similar region ($10 \leq x/H \leq 18$). It is such large set of data that is used in Figs. 2–10, except for Fig. 3 where plotted data pertain to specific x, y values shown separately.

We are looking for closures for tensor-based quantities appearing in Eqs. (20)–(22) and these will necessarily involve coefficients which can be independent of the component (isotropic) or not (anisotropic). Both types of coefficient will be investigated here through the *a priori* testing, but when analyzing the isotropic coefficients we will rely on a governing equation for the filtered trace of the conformation tensor, as was done previously by Ferreira *et al.*³⁷ for forced homogeneous isotropic turbulence (FHIT). Additionally, for conciseness, when analyzing some SGS terms we will also show plots involving the corresponding quantities from the filtered trace equation. The equation for the evolution of the filtered trace of the conformation tensor can be written as

$$\underbrace{\frac{\partial \bar{C}_{ii}}{\partial t}}_{C_t} + \underbrace{\bar{u}_k \frac{\partial \bar{C}_{ii}}{\partial x_k}}_{C_a} = 2 \underbrace{\frac{\partial \bar{u}_i}{\partial x_k} \bar{C}_{ik}}_{C_p} - \frac{1}{\lambda} \left[\underbrace{f(\bar{C}_{kk}) \bar{C}_{ii} + \chi_{ii}}_{C_d} - \delta_{ii} \right] - \psi_{ii} + \gamma_{ii}, \quad (29)$$

where C_t and C_a are the temporal and advection terms while C_p and C_d are the production and dissipation of the trace of the filtered conformation tensor components (\bar{C}_{ii}), respectively. The two remaining terms on the RHS of Eq. (29), ψ_{ii} and γ_{ii} , are the unknown subgrid-

TABLE I. Summary of physical and computational parameters of the DNS used to perform *a priori* tests, extracted from Guimarães *et al.*⁴⁷. $A_\delta, A_{U_c},$ and A_{τ_c} are slopes of the laws of variation of jet width (δ), mean centerline velocity (U_c), and centerline stress (τ_c) discussed later, domain size $\frac{L_x \times L_y \times L_z}{H^3} = 18 \times 18 \times 4.5$.

	Wi	λ (s)	β_s	L	Grid points	A_δ	A_{U_c}	A_{τ_c}
DNS _N	0	0	1.0	NA	$512 \times 512 \times 128$	0.110	0.21	NA
DNS _{1.1}	1.1	0.4	0.8	100	$512 \times 512 \times 128$	0.111	0.208	1.40
DNS _{2.2}	2.2	0.8	0.8	100	$512 \times 512 \times 128$	0.095	0.176	0.56
DNS _{3.3}	3.3	1.2	0.8	100	$512 \times 512 \times 128$	0.080	0.141	0.37

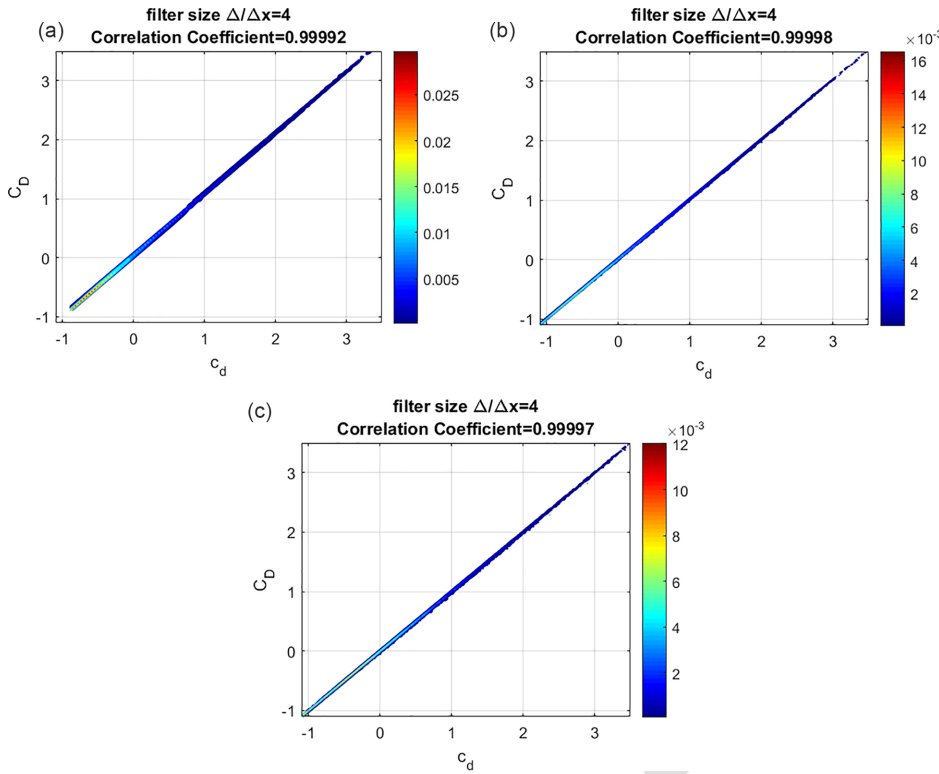


FIG. 2. Joint Probability density function (JPDF) of $c_d = \overline{f(C_{kk})}C_{ij}$ and $C_D = \overline{f(C_{kk})}C_{ij}$ normalized by their root mean square obtained from DNS at (a) $Wi = 1.1$, (b) 2.2, and (c) 3.3 with a filter size $\Delta/\Delta x = 4$. All data are from the jet centerline ($y/H = 0$) in the range $10 \leq x/H \leq 18$. Lines are a guide to the eye.

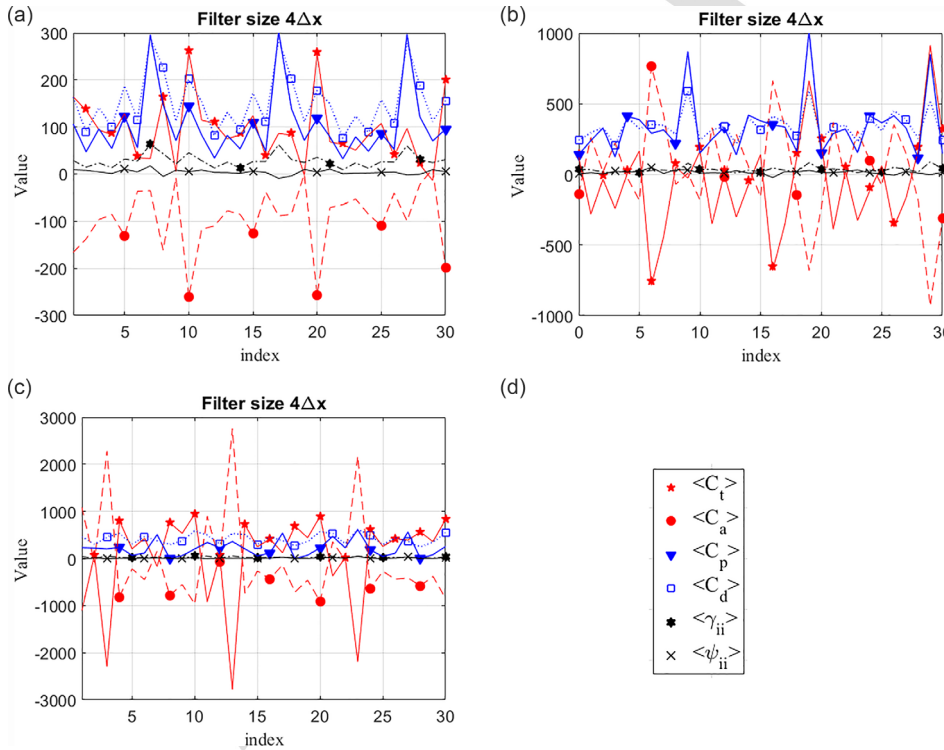


FIG. 3. The variation of terms in Eq. (29), averaged in the homogeneous direction, at a number of points (30) on the jet centerline ($y/H = 0$) for $10 \leq x/H \leq 18$. The DNS data pertain to (a) $Wi = 1.1$, (b) 2.2, and (c) 3.3. The legend is shown as part (d), the filter size was $\Delta/\Delta x = 4$ and the key to the plotted quantities is shown at the top of (a). Lines are a guide to the eye.

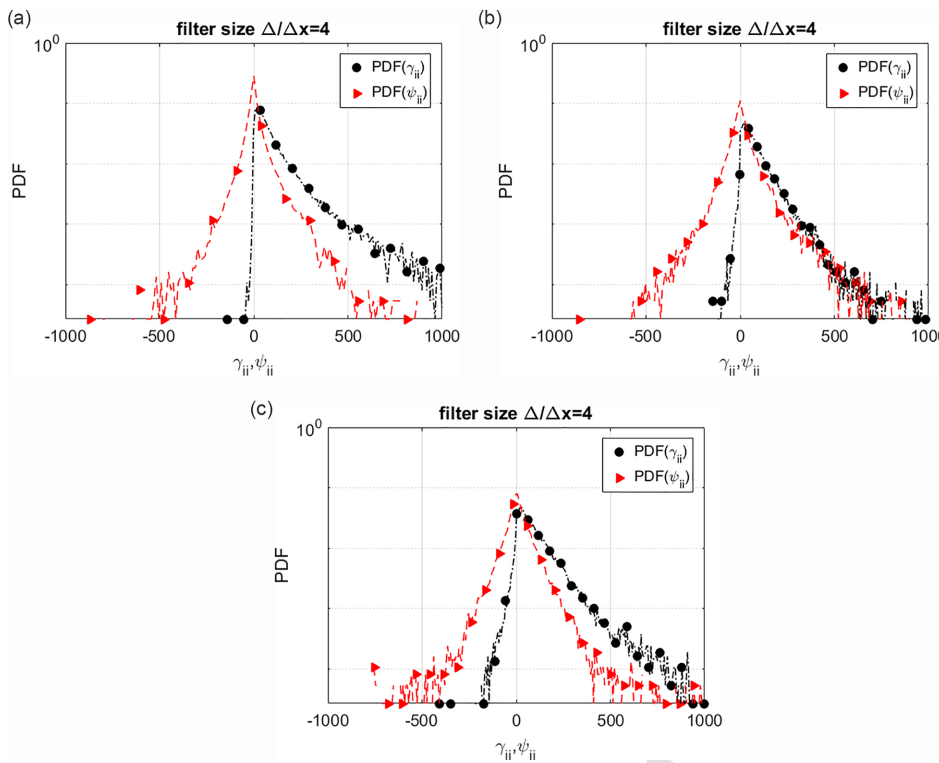


FIG. 4. PDF of the SGS of both advection of the trace of the conformation tensor and polymer stretching terms, obtained from DNS at (a) $Wi = 1.1$, (b) 2.2, and (c) 3.3 with a filter size $\Delta/\Delta x = 4$. All data are from the jet centerline ($y/H = 0$) in the range $10 \leq x/H \leq 18$. Lines are a guide to the eye.

497 scale contributions from the advection and polymer stretching, respec- 518
 498 tively, and χ_{ii} represents the SGS contribution to the dissipation of 519
 499 elastic energy. 520

500 Next, a series of six hypothesis will be tested in order to develop 521
 501 the closures needed by the filtered governing constitutive equation. 522

502 **A. SGS of polymer dissipation: Hypothesis H1** 523

503 The first hypothesis (H1) deals with the filtered nonlinear conforma- 524
 504 tion tensor term (χ_{ij}) in the filtered conformation tensor evolution 525
 505 equation and in Eqs. (16)–(18) for the filtered polymer stress, which 526
 506 needs to be assessed in order to develop a LES closure.^{36,45} The term 527
 507 can be decomposed as on the left side of the arrow in Eq. (30), where 528
 508 the difference inside the parentheses is the SGS contribution. The 529
 509 hypothesis is that the SGS term is very small and can be neglected; 530
 510 therefore, the filtered term equals the GS contribution as on the right- 531
 511 hand-side of the arrow in the following:

$$\begin{aligned} \overline{f(C_{kk})C_{ij}} &= f(\overline{C_{kk}})\overline{C_{ij}} + \underbrace{\left(\overline{f(C_{kk})C_{ij}} - f(\overline{C_{kk}})\overline{C_{ij}} \right)}_{\chi_{ij}} \\ &\rightarrow \overline{f(C_{kk})C_{ij}} \approx f(\overline{C_{kk}})\overline{C_{ij}} \text{ or } \chi_{ij} \approx 0. \end{aligned} \quad (30)$$

512 Note that in homogeneous flows and considering the filtering proper- 532
 513 ties for a box filter, one concludes that $\overline{f(C_{kk})} = f(\overline{C_{kk}})$. Even though 533
 514 the jet flow is not homogeneous, this equality will still be assumed. 534

515 Figures 2(a)–2(c) show the joint probability density function 535
 516 (JPDF) of the $c_d = f(C_{kk})C_{ii}$ and $C_D = f(C_{kk})\overline{C_{ii}}$ in the viscoelastic 536
 517 turbulent planar jet flow for $Wi = 1.1, 2.2, 3.3$ and for a filter size equal 537

to $\Delta/\Delta x = 4$ (for filter sizes $\Delta/\Delta x = 2$ and 8 similar results are 518
 observed). The two quantities are strongly correlated, and the correla- 519
 tion coefficient is very close to 1, which means that the two quantities 520
 are closely matched. Note that the JPDF plotted involves the trace of 521
 the conformation tensor (C_{ii}), but hypothesis (H1) remains valid if the 522
 sink terms are assessed individually. These are not shown for conciseness. 523
 Masoudian *et al.*⁴⁶ and Ferreira *et al.*³⁷ reached similar results for 524
 turbulent channel flow and forced isotropic turbulence of FENE-P fluids, 525
 respectively. The results in Fig. 2 confirm the validity of assumption 526
 H1 for a free flow in the presence of mean shear. Therefore, this 527
 assumption is used henceforth in the present study. 528

529 **B. SGS of advection: Hypothesis H2** 530

531 The second hypothesis (H2) deals with the subgrid-scale advec- 532
 tion and we analyze next the corresponding term for the trace of the 533
 filtered conformation tensor, denoted ψ_{ii} , and defined according to 534
 Eq. (21). 535

536 Hypothesis H2 assumes that the SGS contribution of the advec- 537
 tion from the filtered conformation tensor equation is negligible when 538
 compared with the resolved advection term. Figures 3(a)–3(c) plot the 539
 variations of all terms of Eq. (29) averaged in the homogeneous direc- 540
 tion; as shown $\langle \psi_{ii} \rangle$ is much smaller than the other quantities and, in 541
 particular, smaller than $\langle C_a \rangle$. In Fig. 3, we consider data at an instant 542
 of time at specific (x, y) points on the jet centerline, but within the 543
 self-similarity region. Each data point marked in the abscissa actually 544
 corresponds to the average of the 128 points in the homogeneous 545
 z -direction of the domain (at that value of (x, y)), i.e., in contrast to 546
 the figures showing the joint PDFs, we are not mixing data at all 547

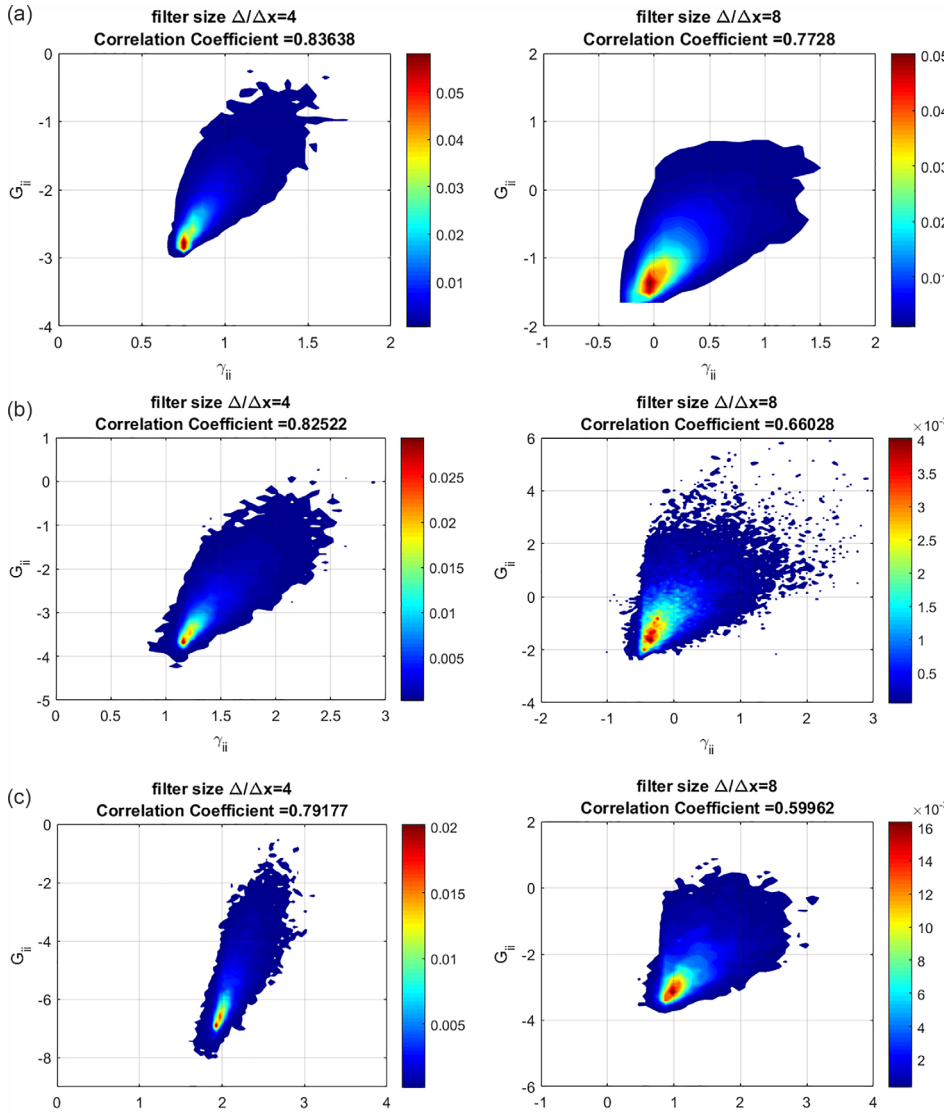


FIG. 5. JPDF between the trace of SGS polymer stretching terms γ_{ii} and G_{ii} normalized by their root mean square obtained from DNS at (a) $Wi = 1.1$, (b) 2.2, and (c) 3.3 with filter sizes $\Delta/\Delta x = 4$ (left column) and $\Delta/\Delta x = 8$ (right column). All data are from the jet centerline ($y/H = 0$) in the range $10 \leq x/H \leq 18$. Lines are a guide to the eye.

545 points. For clarity, only data from 30 (x, y) points are shown, but we
 546 observe a similar behavior when considering all points in that region.
 547 It is not shown here for conciseness, but hypothesis H2 remains valid
 548 when comparing individually $\langle \psi_{ij} \rangle$ with $\langle C_{a_{ij}} \rangle$.

549 Figures 4(a)–4(c) show the probability density function (PDF) of
 550 ψ_{ii} and γ_{ii} at the self-similar region of the turbulent viscoelastic jet for
 551 $Wi = 1.1, 2.2, 3.3$, respectively, for a filter size equal to $\Delta/\Delta x = 4$.
 552 These confirm that locally, the quantities of $\psi_{ii} \ll \gamma_{ii}$. As shown, the
 553 skewness of γ_{ii} is also significantly more intense than that of ψ_{ii} , so
 554 $\langle \gamma_{ii} \rangle_{z\text{-direction}} \neq 0$, whereas $\langle \psi_{ii} \rangle_{z\text{-direction}} \approx 0$. Masoudian *et al.*⁴⁶ and
 555 Ferreira *et al.*³⁷ also reported that ψ_{ii} is negligible in DNS of turbulent
 556 channel flows and forced isotropic turbulence of FENE-P fluids,
 557 respectively. Therefore, the comparison shows that the SGS of polymer
 558 stretching γ_{ii} , or γ_{ij} cannot be ignored.

559 It is also observed in Fig. 4 that by increasing Wi , not only the
 560 skewness of the polymer stretching SGS, but also the tendency of

having negative quantities of it, both increase. The same behavior was 561
 observed and reported by Ferreira *et al.*³⁷ and interpreted there as a 562
 sign of the formation of the polymer induced energy cascade at larger 563
 Wi number, which was explained in detail by Ref. 40. 564

C. Scale-similarity of the subgrid-scale polymer stretching: Hypothesis H3 565

566 One of the main characteristics of turbulent flows is the existence 567
 of self-similarity in the inertial range of scales, which allows the com- 568
 putation of a given subgrid-scale quantity by assessing the same quan- 569
 tity defined at a nearby scale.⁶⁶ This assumption has been previously 570
 used in the development of many SGS models for Newtonian turbu- 571
 lent flows²⁸ and prompted Ferreira *et al.*³⁷ to develop the DSIM model 572
 for γ_{ij} in Eq. (22) in isotropic turbulence by applying this concept to 573
 the computation of the SGS polymer stretching term. It is important 574

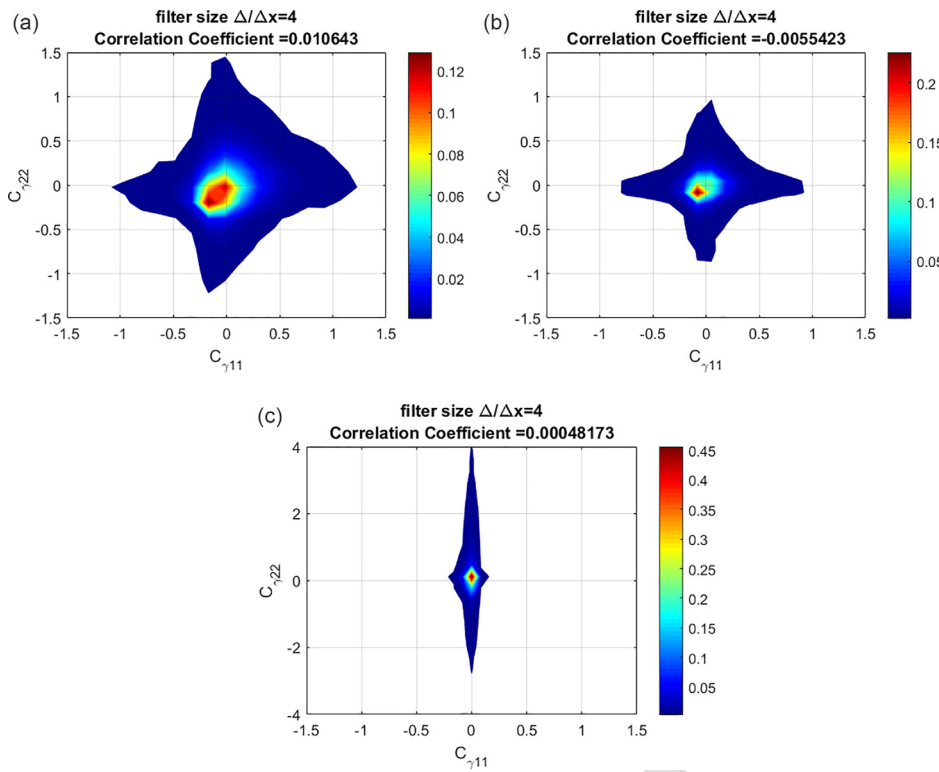


FIG. 6. JPDF between the $C_{\gamma 11}$ and $C_{\gamma 22}$ [calculated from Eq. (34)] obtained from DNS at (a) $Wi = 1.1$, (b) 2.2, and (c) 3.3 with a filter size $\Delta/\Delta x = 4$. All data are from the jet centerline ($y/H = 0$) in the range $10 \leq x/H \leq 18$. Lines are a guide to the eye.

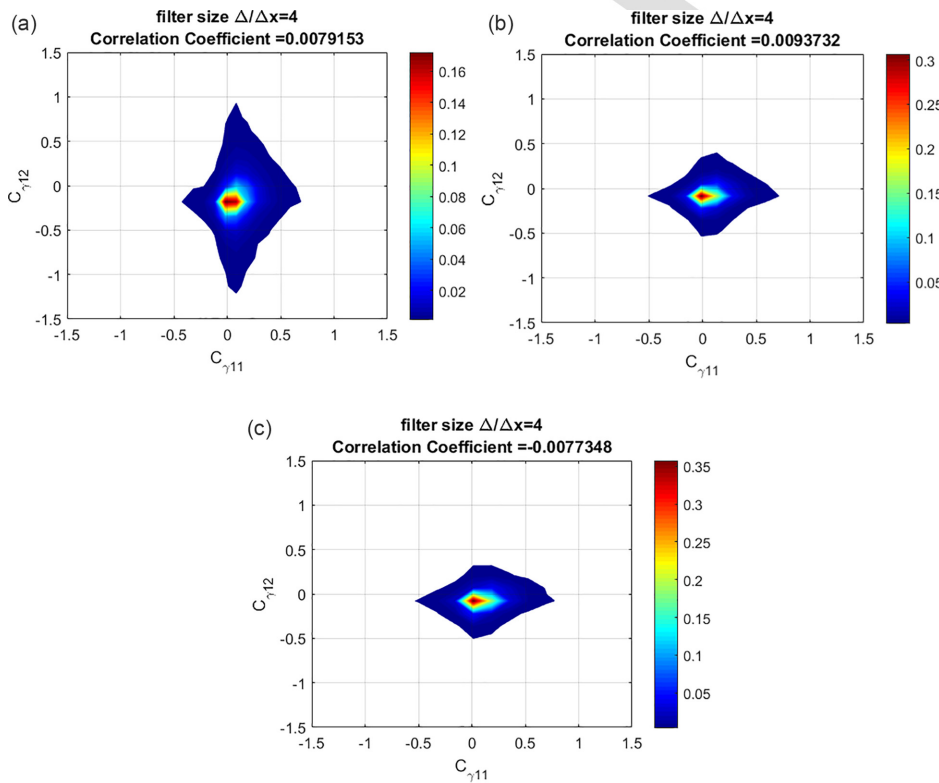


FIG. 7. JPDF between the $C_{\gamma 11}$ and $C_{\gamma 12}$ [calculated from Eq. (34)] obtained from DNS at (a) $Wi = 1.1$, (b) 2.2, and (c) 3.3 with a filter size $\Delta/\Delta x = 4$. All data are from the jet centerline ($y/H = 0$) in the range $10 \leq x/H \leq 18$. Lines are a guide to the eye.

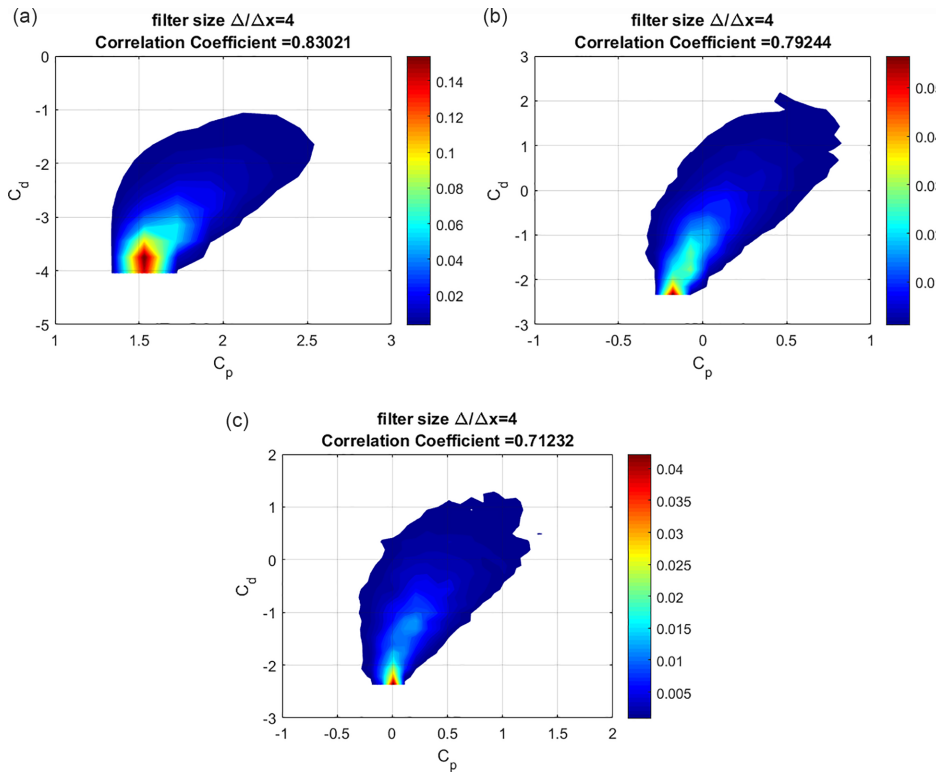


FIG. 8. JPDF functions between polymer stretching C_p and dissipation C_d terms of the trace of the filtered conformation tensor evolution equation obtained from DNS at (a) $Wi = 1.1$, (b) 2.2, and (c) 3.3 with a filter size $\Delta/\Delta x = 4$. All data are from the jet centerline ($y/H = 0$) in the range $10 \leq x/H \leq 18$. Lines are a guide to the eye.

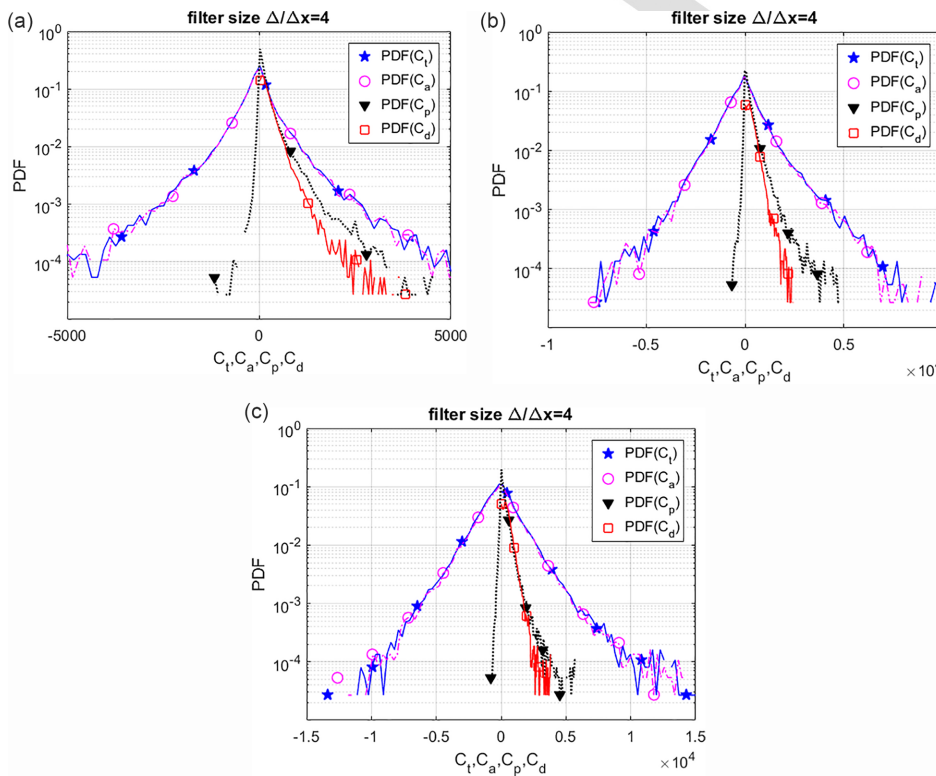


FIG. 9. PDF of the traces of C_t , C_a , C_p , and C_d at (a) $Wi = 1.1$, (b) 2.2, and (c) 3.3 for a filter size $\Delta/\Delta x = 4$. All data are from the jet centerline ($y/H = 0$) in the range $10 \leq x/H \leq 18$. Lines are a guide to the eye.

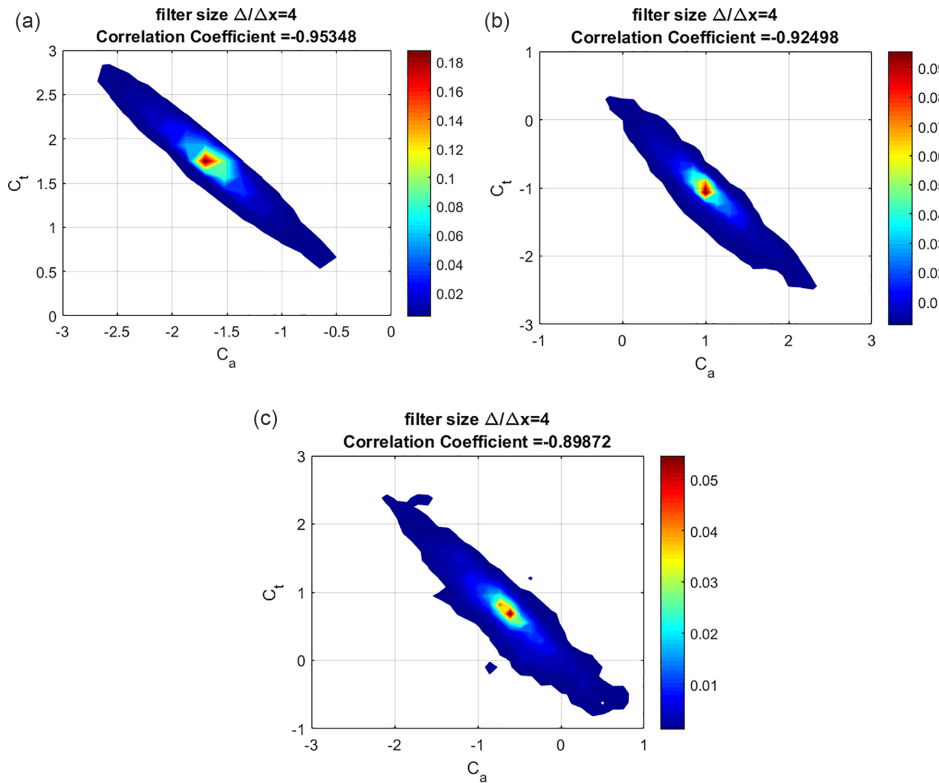


FIG. 10. JPDF functions between temporal C_t and advection C_a terms from the trace of the conformation tensor transport, obtained from DNS at (a) $Wi = 1.1$, (b) 2.2, and (c) 3.3 with a filter size $\Delta/\Delta x = 4$. All data are from the jet centerline ($y/H = 0$) in the range $10 \leq x/H \leq 18$. Lines are a guide to the eye.

575 to assess this assumption in the present inhomogeneous flow configura-
 576 tion. Specifically, the self-similarity of subgrid-scales was originally
 577 proposed by Bardina *et al.*,⁶⁷ for the SGS stress tensor of the momen-
 578 tum equation. The model assumes that the SGS stress (for a
 579 Newtonian fluid) can be approximated by

$$\tau_{ij}^{sgs} = c(\widetilde{\widetilde{u_i u_j}} - \widetilde{u_i} \widetilde{u_j}), \quad (31)$$

580 where C is a constant of order $O(1)$, and $\widetilde{\Delta}$ is the width of the test filter,
 581 often taken as having of twice the width of the original filter. By applying
 582 this concept to the subgrid-scale polymer stretching term [γ_{ij} in Eq.
 583 (22)], the subgrid-scale polymer stretching at the test filter width is

$$G_{ij} = \left[\frac{\partial \widetilde{u_j}}{\partial x_k} C_{jk} - \partial \widetilde{u_i} \right] + \left[\frac{\partial \widetilde{u_j}}{\partial x_k} C_{ik} - \partial \widetilde{u_j} \right]. \quad (32)$$

584 By considering the self-similarity of the subgrid-scales computed at fil-
 585 ter widths Δ and $\widetilde{\Delta}$, (here we take $\widetilde{\Delta} = 2\Delta$) the SGS of polymer
 586 stretching tensor is calculated by

$$\gamma_{ij} = C_\gamma G_{ij}, \quad (33)$$

587 where C_γ is a numerical coefficient that needs to be computed. This
 588 constitutes the assumption **H3** used by Ferreira *et al.*³⁷ in homo-
 589 geneous turbulence.

590 To assess this assumption in the turbulent jet flow configuration,
 591 Figs. 5(a)–5(c) show the joint probability density functions (JPDFs) of

the trace of the SGS polymer stretching terms γ_{ii} and G_{ii} with $Wi = 1.1, 2.2,$ and 3.3 and for filter size $\Delta/\Delta x = 4$ and 8 .

The two quantities are clearly correlated, and the correlation coefficient between γ_{ii} and G_{ii} varies between 0.83 and 0.599, so of order 1, depending on the filter size and Wi number. Specifically, the correlation coefficient decreases when increasing Wi and the filter size, which is similar to the behavior and values described in Ferreira *et al.*³⁷ The correlation coefficients and shape of the PDFs attest that the scale-similarity assumption (**H3**) is also valid for inhomogeneous free shear flows and can be used in the development of SGS closures.

The closure in Eq. (31) has the same coefficient for all tensor components, i.e., it is an isotropic model, still to be determined. As in Ferreira *et al.*³⁷ we now investigate the possibility of using anisotropic model coefficients $C_{\gamma_{ij}}$, defined by a rewriting of assumption **H3** as

$$\gamma_{ij} = C_{\gamma_{ij}} G_{ij} \text{ (no summation on } i \text{ and } j). \quad (34)$$

To investigate this issue, Figs. 6 and 7 show the JPDF between $C_{\gamma_{11}} = \frac{\gamma_{11}}{G_{11}}$ and $C_{\gamma_{22}} = \frac{\gamma_{22}}{G_{22}}$, and between $C_{\gamma_{11}} = \frac{\gamma_{11}}{G_{11}}$ and $C_{\gamma_{12}} = \frac{\gamma_{12}}{G_{12}}$, respectively, for filter size $\Delta/\Delta x = 4$.

As in Ferreira *et al.*³⁷ for homogeneous turbulence, the figures clearly show that the correlation coefficients between $C_{\gamma_{11}}$ and $C_{\gamma_{22}}$ and between $C_{\gamma_{11}}$ and $C_{\gamma_{12}}$ are approximately zero. This means that these quantities are statistically independent, which validates the assumption of using an isotropic C_γ in the DSIM SGS model, also for the inhomogeneous flow configuration used in the present work. For other combinations of coefficients not shown, the correlation coefficient was equally very small.

617 D. Local equilibrium of the polymeric elastic energy
618 and statistically stationary flow: Hypothesis H4, H5,
619 and H6

620 We now investigate the hypothesis used by Ferreira *et al.*³⁷ to
 621 compute the model constant C_γ , defined in Eq. (34). By using Eq. (29)
 622 and by employing the condition of statistical stationarity and homoge-
 623 neity Ferreira *et al.*³⁷ arrived at the following expression:

$$\left\langle \frac{\partial \overline{u_i}}{\partial x_k} \overline{C_{ik}} \right\rangle = \left\langle \frac{1}{\lambda} \left[\overline{f(C_{kk})} \overline{C_{ii}} - \delta_{ii} \right] \right\rangle, \quad (35)$$

624 where the brackets $\langle \rangle$ denote an ensemble averaging operation which
 625 was performed in all three homogeneous directions in the homoge-
 626 neous isotropic turbulence configuration of Ferreira *et al.*³⁷ In such
 627 context, this expression represents the “global” equilibrium of the
 628 resolved elastic energy, i.e., in statistically stationary isotropic turbu-
 629 lence the elastic energy produced by the interaction between the poly-
 630 mer molecules and the turbulent velocity fluctuations is balanced by
 631 its transfer into the polymer molecules where it is stored as elastic
 632 energy, so that the total (resolved) elastic energy—which is proportional
 633 to $\overline{C_{kk}} = \overline{C_{xx}} + \overline{C_{yy}} + \overline{C_{zz}}$ —remains constant. We denote this assump-
 634 tion as **H4**.

635 It is important to clarify how this assumption can be used in the
 636 context of the present flow configuration since it is clear that in turbu-
 637 lent jet flows, as well as in other inhomogeneous flow configurations,
 638 Eq. (35) will not be exactly verified. Hence, one needs to assess how
 639 this expression, or some sort of variant of it, can be used in order to
 640 extend the DSIM model into free shear flows.

641 We start by noting that statistical stationarity in the far field (fully
 642 developed) region of the jet allows one to write also

$$\left\langle \frac{\partial \overline{C_{ii}}}{\partial t} \right\rangle = 0, \quad (36)$$

643 (we denote this assumption by **H5**). The brackets still refer to averag-
 644 ing in the homogeneous direction, which in the present context is the
 645 z -direction. By averaging Eq. (29) and considering a negligible $\langle \psi_{ii} \rangle$
 646 (**H2**), together with the self-similarity assumption for the SGS polymer
 647 stretching term (**H3**), this equation can be written as

$$\left\langle \overline{u_k} \frac{\partial \overline{C_{ii}}}{\partial x_k} \right\rangle = \left\langle 2 \frac{\partial \overline{u_i}}{\partial x_k} \overline{C_{ik}} \right\rangle - \left\langle \frac{1}{\lambda} \left[\overline{f(C_{kk})} \overline{C_{ii}} - \delta_{ii} \right] \right\rangle - \langle C_\gamma G_{ii} \rangle. \quad (37)$$

648 Notice that the term on the LHS of Eq. (37) is the mean advection of
 649 the trace of the conformation tensor, which is rigorously zero in isotropic
 650 turbulence due to the homogeneity of the flow, but has to be
 651 retained in inhomogeneous turbulent flows, such as in turbulent visco-
 652 elastic jets. However, it is likely that this term is negligible compared to
 653 the other terms. Indeed, whereas the advection of $\overline{C_{ii}}$ is clearly associ-
 654 ated with the largest scales of motion in the jet, the terms representing
 655 the production and dissipation of $\overline{C_{ii}}$ —the first and second terms on
 656 the RHS of Eq. (37)—are governed by the smallest scales of the flow.
 657 We denote this assumption (neglecting the advection of $\overline{C_{ii}}$) by **H6**.
 658 We can therefore use an expression similar to the one used by Ferreira
 659 *et al.*³⁷ for the determination of the model constant C_γ , with only
 660 minor corrections related to the averaging procedure.

661 By inserting all the aforementioned hypotheses into Eq. (37), the
 662 model constant C_γ can be obtained from the following expression:

$$C_\gamma = \frac{\left\langle \frac{1}{2\lambda} \left[\overline{f(C_{kk})} \overline{C_{ii}} - \delta_{ii} \right] \right\rangle_z - \left\langle \frac{\partial \overline{u_i}}{\partial x_k} \overline{C_{ik}} \right\rangle_z}{\left\langle \frac{\partial \overline{u_i}}{\partial x_k} \overline{C_{ik}} - \frac{\partial \overline{u_i}}{\partial x_k} \overline{C_{ik}} \right\rangle_z}, \quad (38)$$

663 where the averaging procedure now consists on a spatial average car-
 664 ried out along the only flow direction where the flow is homogeneous
 665 (z -direction).

666 Hypothesis **H5** does not need to be assessed as it stems directly
 667 from the concept of statistical stationarity, whereas hypothesis **H4** and
 668 **H6** are somehow related and need to be assessed simultaneously.

669 In order to assess hypothesis **H4–H6** dealing with local equilib-
 670 rium assumption, Fig. 8 shows the joint probability density functions
 671 (JPDFs) of the polymer stretching (C_p) and dissipation (C_d) of the
 672 trace of the conformation tensor defined in Eq. (29), for $Wi = 1.1, 2.2,$
 673 and 3.3 and filter size $\Delta/\Delta x = 4$. The correlation coefficients between
 674 C_p and C_d are very high, with $0.84, 0.79,$ and 0.71 for $Wi = 1.1, 2.2,$
 675 and 3.3 , respectively, with $\Delta/\Delta x = 4$. This confirms that, as in isotropic
 676 turbulence, C_p and C_d are in approximately local equilibrium, even
 677 though the correlation coefficient slightly decreases with increasing Wi
 678 numbers.

679 To complete the assessment of the **H4–H6** assumptions, it is
 680 important to shown that the other terms of Eq. (29) (terms C_t and C_a)
 681 are negligible in comparison with C_p and C_d terms.

682 Figure 9 shows the probability distribution functions of all terms
 683 of Eq. (29) ($C_t, C_a, C_p,$ and C_d) for $\Delta/\Delta x = 4$ and $Wi = 1.1, 2.2,$
 684 and 3.3 . The PDF of C_t and C_a is symmetric which explains why the local
 685 value of the sum of these quantities is approximately 0. Finally, Fig. 10
 686 shows the joint probability density functions between temporal varia-
 687 tion C_t and advection terms C_a of the trace of the conformation tensor,
 688 for $Wi = 1.1, 2.2,$ and 3.3 and filter size $\Delta/\Delta x = 4$. The correlation
 689 coefficient between C_t and C_a is equal to $-0.95, -0.94,$ and $-0.92,$
 690 which finally confirms that all hypotheses **H4, H5,** and **H6** are
 691 verified.

692 To summarize, all the *a priori* tests conducted in the reference
 693 DNS of turbulent viscoelastic jets clearly show that all the assumptions
 694 used by Ferreira *et al.*³⁷ in the development of the DSIM model in iso-
 695 tropic turbulence are also valid in the present inhomogeneous free tur-
 696 bulent flow configuration, and are likely valid in other free shear flows
 697 of viscoelastic fluids such as wakes and mixing layers. In Sec. VI,
 698 we assess the combination of all closures through a *posteriori* (LES) tests.

699 VI. A POSTERIORI TESTS: LES OF TURBULENT PLANAR
700 JET FENE-P FLUID

701 Several LES of turbulent planar jet flow of FENE-P fluid were
 702 performed with the various closures presented, including the
 703 Smagorinsky and dynamic Smagorinsky models for SGS term of
 704 momentum equation and the DSIM model for the SGS polymer
 705 stretching term in the conformation tensor equation. The results are
 706 assessed against the reference DNS of Guimarães *et al.*⁴⁷ in what are
 707 typically called *a posteriori* tests. The comparisons confirm that the
 708 DSIM model, in its original formulation and, in particular, in combi-
 709 nation with the dynamic Smagorinsky closure for the SGS stress, per-
 710 forms well in planar turbulent jets, and arguably the same should be
 711 true for other free shear flows. Incidentally, we did also some tests
 712 using the Vreman⁶⁸ and the shear improved Smagorinsky⁶⁹ closures
 713 for the SGS stress, but no advantages were observed relative to the

AQ4

714 dynamic Smagorinsky model; therefore, for the sake of conciseness,
715 such results are neither presented nor those closures introduced.

716 The LES were carried out with the same numerical code used in
717 Guimarães *et al.*⁴⁷ and the physical and computational parameters are
718 chosen as close as possible to those of the reference DNS, naturally
719 using coarser grids than in the DNS.

720 The amplitude of noise for all inlet velocity fluctuations was set at
721 10%, as in Guimarães *et al.*⁴⁷ however, the ratio between the inlet slot-
722 width and momentum thickness was set to $H/\theta = 15$,^{47,49} to avoid the
723 Gibbs phenomena that could arise with the coarser grids used in LES.
724 In the following, we use subscripts “N” (Newtonian fluid), “Sm”
725 (Smagorinsky), and “Dyn” (dynamic Smagorinsky) to denote the vari-
726 ous subgrid-scale stress closures used in the computation. Subscript
727 “f” represents a second LES carried out using a finer grid. The main
728 details of the simulations are summarized in Table II, where the
729 reported values of A_δ , A_{U_c} , A_{σ_c} were obtained using the dynamic
730 Smagorinsky model.

731 In all simulations and similarly to the DNS of Guimarães *et al.*,⁴⁷
732 the Reynolds number was equal to $Re = 3500$, and the ratio of the sol-
733 vent to total viscosity and the maximum dumbbell extensibility were
734 equal to $\beta = 0.8$ and $L^2 = 10^4$, respectively. The domain size was
735 $L_x = 19.2H$, $L_y = 24H$ in the streamwise and normal directions, and
736 $L_z = 6H$ in the spanwise direction, for a “normal” grid size with
737 $192 \times 192 \times 48$ grid points, and a “finer” grid size with $256 \times 256 \times 64$
738 points. By considering $\lambda = 0.3, 0.6, 0.9$ s, the global Weissenberg
739 number became equal to $Wi = 1.1, 2.2, 3.3$.

740 A. Instantaneous vorticity and trace of conformation 741 tensor field

742 Figures 11(a)–11(d) show contours of instantaneous vorticity
743 magnitude normalized by $(U_j - U_\infty^{in})/H$ in the (x, y) plane of the tur-
744 bulent planar jet obtained by LES for Newtonian and viscoelastic flows
745 at Weissenberg numbers, $Wi = 1.1, 2.2, 3.3$. These results were
746 obtained in the finer grid (LES_f) and used the dynamic Smagorinsky
747 model.

748 The Newtonian contours in Fig. 11(a) are very similar to those
749 shown in Guimarães *et al.*,⁴⁷ for the same physical conditions.
750 Kelvin–Helmholtz vortices emerge at about at $x/H \approx 4$ for all simula-
751 tions and tend to break up into smaller-scale eddies after about x/H
752 ≈ 6 . By about $x/H \approx 10$ –12, the flow seems to have attained the typi-
753 cal features of fully developed turbulence, with a clear display of many

TABLE II. Summary of physical and computational features of LES used in the *a posteriori* tests with domain size $\frac{L_x \times L_y \times L_z}{H^3} = 19.2 \times 24 \times 6$.

	Wi	λ (s)	β_s	L	Grid points	A_δ	A_{U_c}	A_{τ_c}
LES _N	0	0	1.0	NA	$192 \times 192 \times 48$	0.124	0.165	NA
LES _{1.1}	1.1	0.3	0.8	100	$192 \times 192 \times 48$	0.108	0.169	1.8
LES _{2.2}	2.2	0.6	0.8	100	$192 \times 192 \times 48$	0.090	0.156	0.63
LES _{3.3}	3.3	0.9	0.8	100	$192 \times 192 \times 48$	0.084	0.155	0.34
LES _{Nf}	0	0	1.0	NA	$256 \times 256 \times 64$	0.124	0.180	NA
LES _{1.1f}	1.1	0.3	0.8	100	$256 \times 256 \times 64$	0.122	0.187	1.65
LES _{2.2f}	2.2	0.6	0.8	100	$256 \times 256 \times 64$	0.094	0.167	0.57
LES _{3.3f}	3.3	0.9	0.8	100	$256 \times 256 \times 64$	0.085	0.154	0.38

small-scale eddies without any preferential direction. As reported by
Guimarães *et al.*⁴⁷ and the other extensive studies on turbulent visco-
elastic fluids,^{70–73} the main effects of increasing the Wi number in the
turbulent planar jet structure are (i) a significant suppression of small-
scale turbulent motions (compared to the Newtonian reference case),
with a concomitant considerable reduction of the vorticity magnitude
as observed by the range of values of $|\omega^+|$ obtained, (ii) the elongation
of the eddy structures, and (iii) a reduction of the jet spreading rate.
All of these features are clearly shown in Fig. 11. The effect of polymers
on the dampening of the vorticity magnitude can be well appreciated
in these figures since increasing Wi from 0 (Newtonian) to 3.3 causes
the maximum vorticity magnitude to decrease from $|\omega^+|_{\max} = 9.15$
for the LES of the Newtonian fluid to 4.55 for the LES of FENE-P fluid.
Simultaneously, the coherent structures become more elongated and
spread at a lower rate. Similar observation were reported in Guimarães
*et al.*⁴⁷ and many experimental studies, e.g., Refs. 74–78.

As the detailed investigations of forced homogeneous isotropic
turbulence have shown^{39,40} the increase in Wi leads to a situation in
which the polymer timescale becomes larger than the Kolmogorov
scale. Further increases in Wi result in a deviation of the large to small
scale turbulent kinetic energy transfer from the classical mechanism to
a polymer induced cascade mechanism. This is seen through both
reductions of vorticity and of small scale turbulent motion (at the
same level of vorticity). As has been previously observed in inhomoge-
neous wall turbulence,^{12,13,70–73} and is also seen in this jet flow,⁴⁷ these
features and the strain hardening of some fluid properties, such as the
fluid extensional viscosity, lead to stronger reductions in transverse
and spanwise turbulence than in streamwise turbulence and the
enhanced turbulence anisotropy translates into more elongated
structures.

Figure 12 shows contours of the trace of conformation tensor
 $\text{tr}(C)$ which is proportional to the elastic energy stored by the stretched
polymer molecules, for $Wi = 1.1, 2.2$, and 3.3 , at the mid-plane of the
computational domain ($z = 0$), and at the same instant of time of Fig.
11. To help the visualizations, the range of the color maps was taken to
be much lower than maximum $\text{tr}(C)$ for all cases. Maxima of $\text{tr}(C)$
occurs in the transitional region, and when approaching the far field
 $\text{tr}(C)$ decreases. Similarly to other studies, e.g., Valente *et al.*³⁹ and
Guimarães *et al.*,⁴⁷ it was observed that even for the most extreme sce-
nario ($Wi = 3.3$), $\text{tr}(C)_{\max} \approx 4500$ in the fully developed turbulence
region (at $x/H \approx 14$) corresponding to $\text{tr}(C)_{\max}/L^2 = 0.45$. However,
inspection of the instantaneous fields shows that the probability of
having local values of $\text{tr}(C)_{\max}/L^2$ is very low, and generally those val-
ues remain $\text{tr}(C)_{\max}/L^2 \ll 1$.

754 B. Classical statistics

In this section, we analyze the statistical quantities obtained from
the several LES carried out with the combined dynamic Smagorinsky
and DSIM models by comparing them with the statistics obtained in
the reference DNS.⁴⁶ In some simulations, the classical Smagorinsky
model was also used. The comparisons are made in terms of
Reynolds-averaged quantities, and for this purpose, the LES and DNS
data of this statistically stationary flow are averaged in time and in
space in the homogeneous direction. To denote Reynolds-averaged
quantities, in this section, we use the overbar, which here does not rep-
resent a filtered quantity.

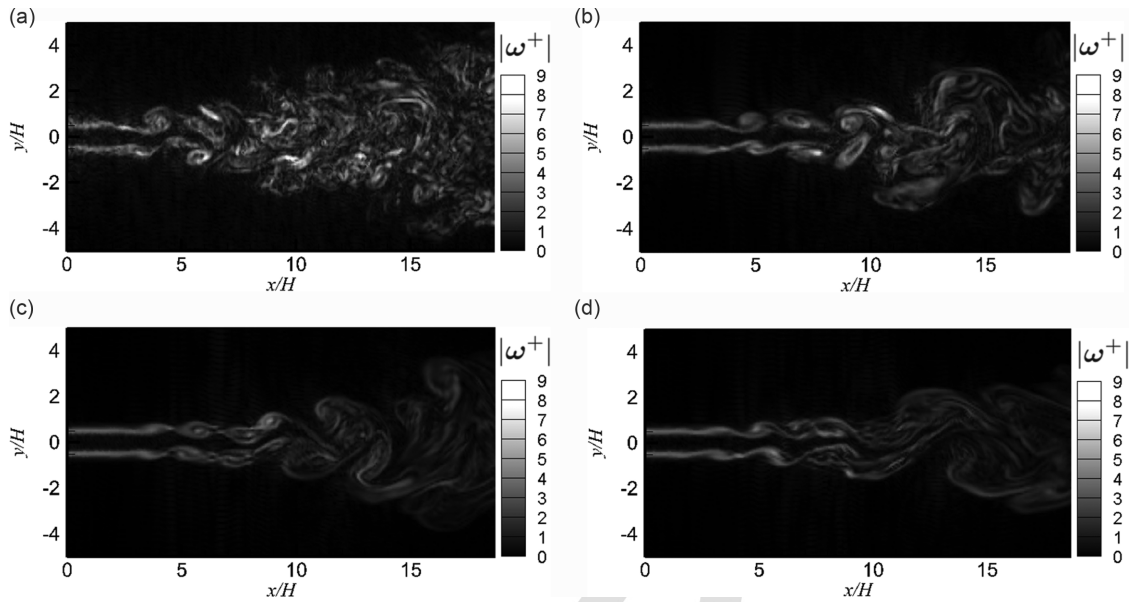


FIG. 11. Contours of instantaneous vorticity normalized by $(U_j - U_\infty^m)/H$ at the middle plane of the domain ($z = 0$) for (a) Newtonian and viscoelastic flows at Wi of (b) 1.1, (c) 2.2, and (d) 3.3. The results were obtained in the finer grid (LES_f) using the dynamic Smagorinsky model.

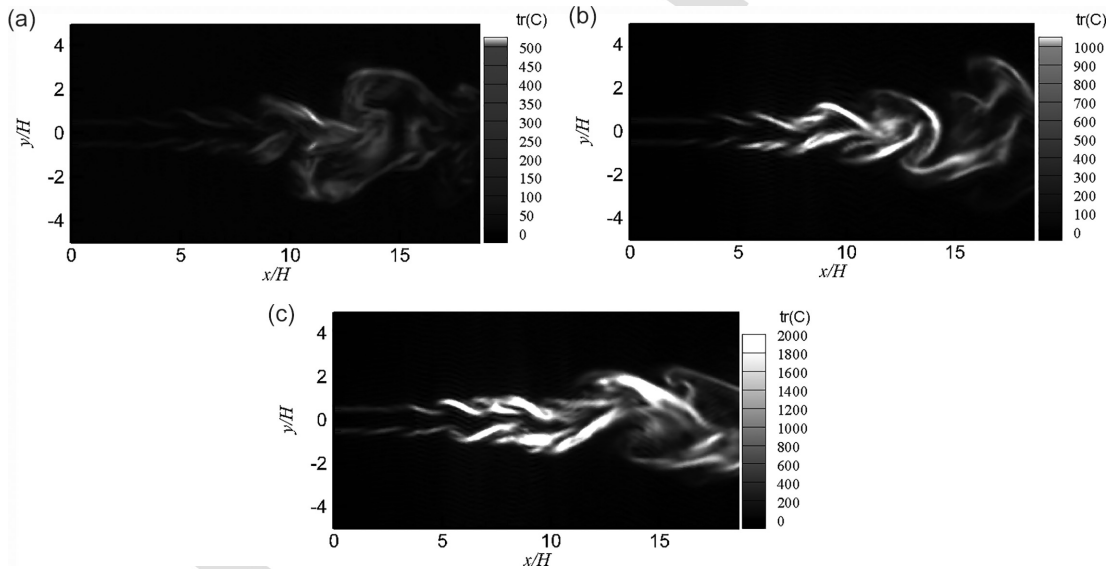


FIG. 12. Contours of the trace of conformation tensor $tr(C)$ for (a) $Wi = 1.1$, (b) 2.2, and (c) 3.3 at the mid-plane of the computational domain ($z = 0$), and corresponding to the same instant of time of Figs. 11(b)–11(d). The results were obtained in the finer grid (LES_f) using the dynamic Smagorinsky model.

809 Guimarães *et al.*⁴⁷ showed that in turbulent viscoelastic jets the
 810 shear layer thickness $\delta(x)$ and the mean centerline velocity decay
 811 $U_c(x)$ evolve as simple functions of the streamwise distance x

$$\frac{\delta(x)}{H} = A_\delta \left(\frac{x - x_0}{H} \right) \quad (39)$$

812 and

$$\left(\frac{U_c(x)}{U_j} \right)^{-2} = A_{U_c} \left(\frac{x - x_0}{H} \right), \quad (40)$$

where A_δ and A_{U_c} are constants and x_0 is the virtual jet origin, and that increasing the Wi number decreases both the shear layer thickness and the centerline velocity decay rates.

Since fluid viscoelasticity and the subgrid-scale models tend to delay the transition to turbulence, the comparison between the

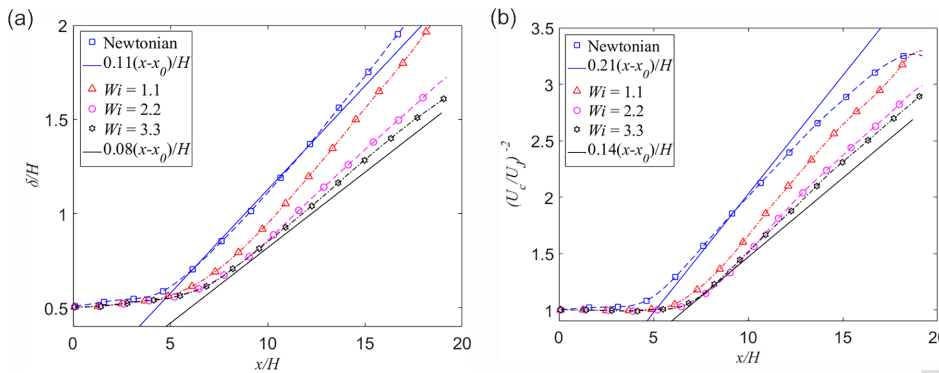


FIG. 13. Evolution of the shear layer thickness (a) and jet centerline velocity decay (b) in LES of turbulent planar jets of Newtonian and FENE-P fluids at $Wi = 1.1, 2.2, 3.3$. Closures used were the dynamic Smagorinsky and DSIM models in the finer grid (LES_{1.1f}, LES_{2.2f}, and LES_{3.3f}) and compared with the reference Newtonian case (LES_{Nf}). Dashed lines connecting symbols are a guide to the eye, and the solid straight lines show the rate laws obtained by DNS at low and high Wi .

818 different models is done through the analysis of the spreading and
 819 decay rates, as measured by A_δ and A_{U_c} , and not through the evolution
 820 of $\delta(x)$ and $U_c(x)$ from the jet inlet.

821 Figures 13(a) and 13(b) show the streamwise variation of the jet
 822 half-width and centerline velocity decay, respectively, for the simula-
 823 tions carried out with the finer grid. The corresponding values of A_δ
 824 and A_{U_c} , in the region $9 \leq x/H \leq 18$, are listed in Table I. The decay
 825 rates A_δ and A_{U_c} for the Newtonian LES (LES_{Nf}) are within the ranges
 826 of $0.092 \leq A_\delta \leq 0.118$ and $0.093 \leq A_{U_c} \leq 0.220$, that have been
 827 reported in previous experimental^{79–83} and numerical (DNS)⁸⁴ studies,
 828 for Newtonian turbulent jets. Regarding the viscoelastic LES and in
 829 agreement with the DNS of Guimarães *et al.*,⁴⁷ the present LES show
 830 that increasing the Weissenberg number postpones the transition to
 831 fully developed turbulence and reduces the values of values A_δ and

A_{U_c} at high Wi . Indeed, up to $Wi = 1.1$, the values of A_δ and A_{U_c}
 remain close to the Newtonian values; however, for $Wi = 2.2$ and 3.3 ,
 both A_δ and A_{U_c} are considerably reduced, while still obeying a linear
 scaling law with $A_\delta = 0.101$, and 0.082 , and $A_{U_c} = 0.171$, and 0.160 ,
 respectively. Moreover, the results are qualitatively consistent with several
 experimental studies, e.g., Refs. 85 and 86.

To study the differences from the SGS model used to compute
 the SGS stresses, Figs. 14 and 15 show the spreading and velocity decay
 rates, respectively, obtained in the LES of the turbulent jet, using the
 classical Smagorinsky and the dynamic Smagorinsky models. It is clear
 that the dynamic Smagorinsky model performs better than the
 Smagorinsky closure, in particular, for the finer grids.

Figures 16(a)–16(c) also analyze the effect of the SGS stress closures
 on the transverse profiles of the normalized mean streamwise

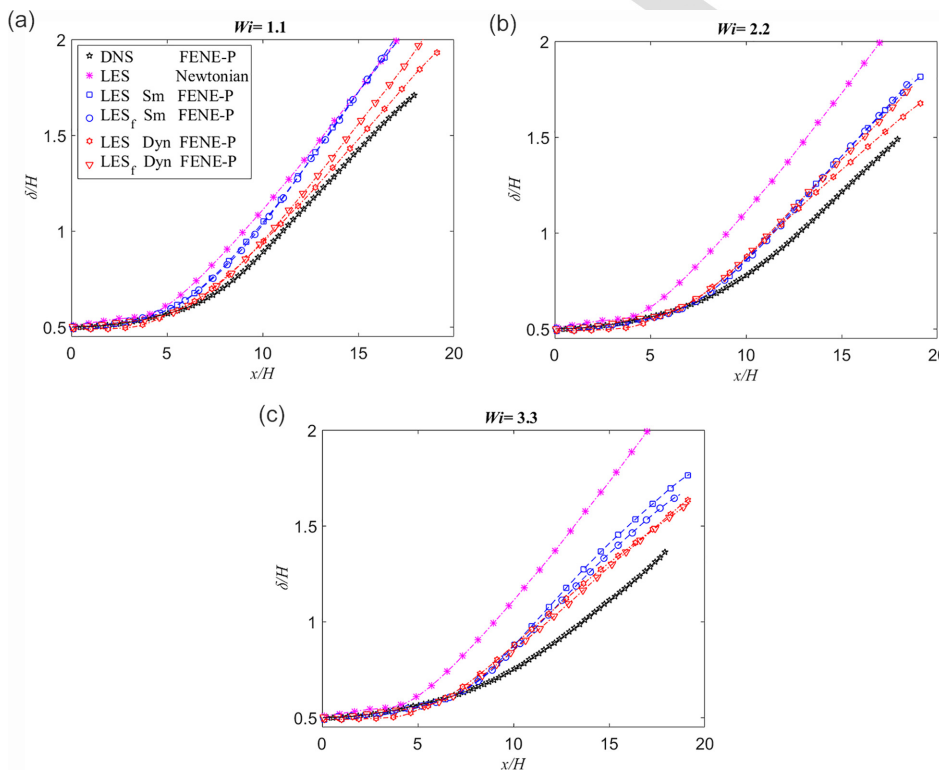


FIG. 14. Effect of the SGS stress model on the evolution of shear layer thickness in the streamwise direction for the turbulent planar jet flows of FENE-P fluid for different SGS stress closures at Wi of (a) 1.1, (b) 2.2, and (c) 3.3. The DSIM closure is used for the SGS polymer stretching in the conformation equation and the Smagorinsky (Sm) and dynamic Smagorinsky (Dyn) for the SGS stress in the momentum equation.

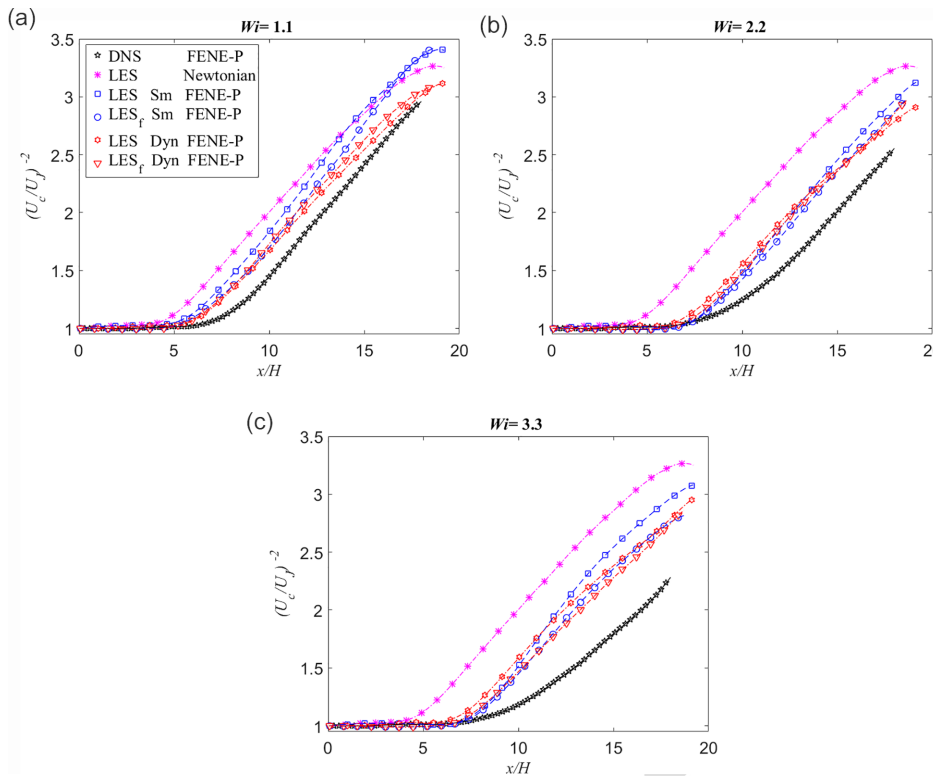


FIG. 15. Effect of SGS stress model on the evolution of jet centerline velocity decay in streamwise direction-planar jet flow of FENE-P fluid for different SGS stress closures at Wi of (a) 1.1, (b) 2.2, and (c) 3.3. The DSIM closure is used for the SGS polymer stretching in the conformation equation and the Smagorinsky (Sm) and dynamic Smagorinsky (Dyn) for the SGS stress in the momentum equation.

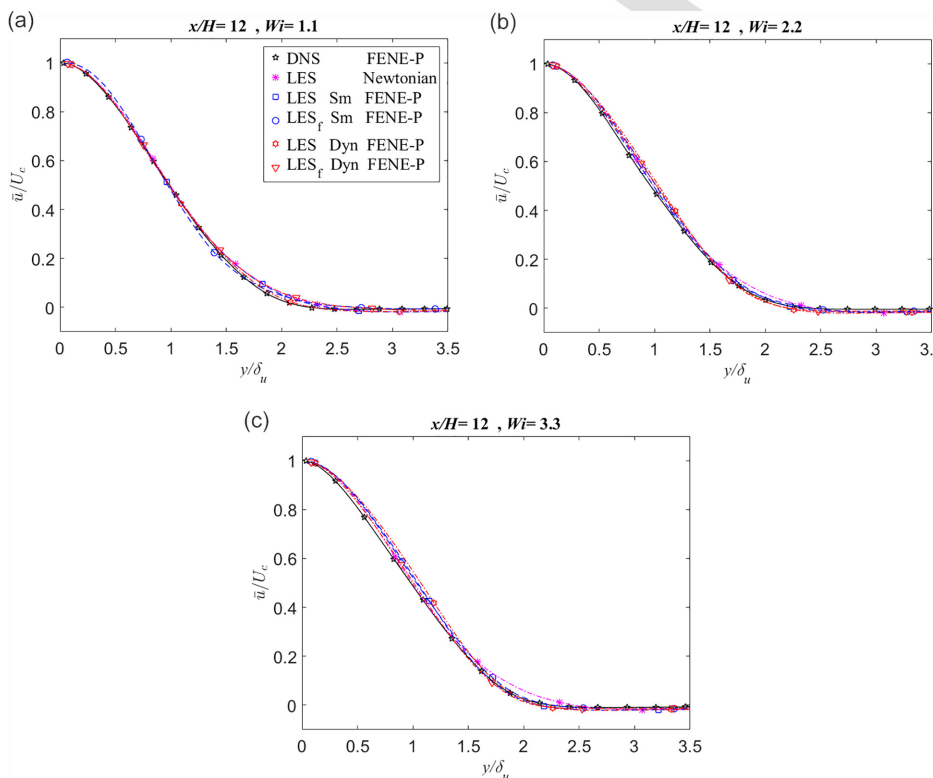


FIG. 16. Effect of SGS stress model on the transverse profiles of streamwise mean velocity normalized by the centerline mean velocity at $x/H = 12$ for Wi of (a) 1.1, (b) 2.2, and (c) 3.3. The DSIM closure is used for the SGS polymer stretching in the conformation equation and the Smagorinsky (Sm) and dynamic Smagorinsky (Dyn) for the SGS stress in the momentum equation.

846 velocity by comparing these profiles at $x/H = 12$ with the results
 847 from the reference DNS. As expected the mean streamwise profiles
 848 collapse, which is consistent in the self-similar region of the flow, but
 849 with the dynamic Smagorinsky closure performing better than the
 850 classical Smagorinsky model (results closer to the DNS data of Ref.
 851 47). Moreover, in agreement with the DNS of Guimarães *et al.*,⁴⁷ the
 852 effect of increasing Wi number on $\bar{u}/U_c(x)$ is negligible.

853 Figures 17–19 show the corresponding streamwise evolutions of
 854 the normal components of the Reynolds stress tensor on the center-
 855 line, here represented as root mean square (rms) of the velocity fluctu-
 856 ations $\sqrt{u'^2}$, $\sqrt{v'^2}$, and $\sqrt{w'^2}$ predicted by LES, and normalized by
 857 the mean centerline velocity $U_c(x)$. The figures include data from the
 858 reference DNS (Guimarães *et al.*⁴⁷). The rms of the velocity fluctu-
 859 ations of LES follow closely the corresponding DNS results, particularly
 860 when the combination of dynamic Smagorinsky and DSIM closures
 861 are used. For $Wi \leq 1.1$, the normal Reynolds stresses gradually increase
 862 along the transition region to a peak at the beginning of the self-
 863 similar region ($x/H \approx 11$), and further downstream their values slightly
 864 decrease as the flow attains the fully developed turbulent flow region.
 865 However, for $Wi \geq 2.2$, the magnitude of the Reynolds stresses
 866 decreases considerably, compared with the turbulent Newtonian jet.
 867 Generally speaking, as reported by Guimarães *et al.*,⁴⁷ the role of the
 868 polymers in the velocity fluctuations can be summarized as postponing
 869 the transition to turbulence and by reducing the Reynolds stresses
 870 in the self-similar region due to depletion of the small scales of motion
 871 caused by a preferential transfer of kinetic energy into the polymer
 872 molecules, instead of the classical multi-scale transfer into the solvent
 873 via the Richardson–Kolmogorov energy cascade. This tendency to the
 874 attenuation of the Reynolds stresses is also reproduced by the present

LES, particularly for the combination of the dynamic Smagorinsky 875
 and the DSIM model. 876

877 Figures 20–22 show the corresponding effects, now on the trans-
 878 verse profiles of the rms of the velocity fluctuations $\sqrt{u'^2}$, $\sqrt{v'^2}$, and
 879 $\sqrt{w'^2}$ predicted by LES. These are normalized by the centerline mean
 880 velocity $U_c(x)$, and the reference DNS profiles are also shown. In the
 881 self-similar region ($x/H = 12$), the rms profiles do not collapse as
 882 seen previously with the mean velocity profiles, but are close to the
 883 DNS profiles, in particular when relying on the dynamic Smagorinsky
 884 for the SGS stress. In all cases the DSIM closure was used for the SGS
 885 stretching term in the constitutive equation.

886 **C. Assessment of the self-similar theory of viscoelastic**
 887 **turbulent planar jets**

888 In this section, we assess the performance of LES in the reproduc-
 889 tion of the main theoretical results derived by Guimarães *et al.*⁴⁷ for
 890 the far field region of viscoelastic turbulent planar jets. In their theory,
 891 Guimarães *et al.*⁴⁷ considered Townsend’s hypothesis of self-preservation
 892 together with the ideas put forward by Lumley⁸⁸ to describe the
 893 flow features of turbulent flows of viscoelastic fluids. In short,
 894 Lumley⁸⁸ defines characteristic velocity (u^*) and length (r^*) scales,
 895 defined as

$$u^* = \sqrt{\lambda \varepsilon^s}, \tag{41}$$

$$r^* = \sqrt{\lambda^3 \varepsilon^s}, \tag{42}$$

where ε^s is the mean viscous dissipation rate of the solvent calculated 896
 by 897

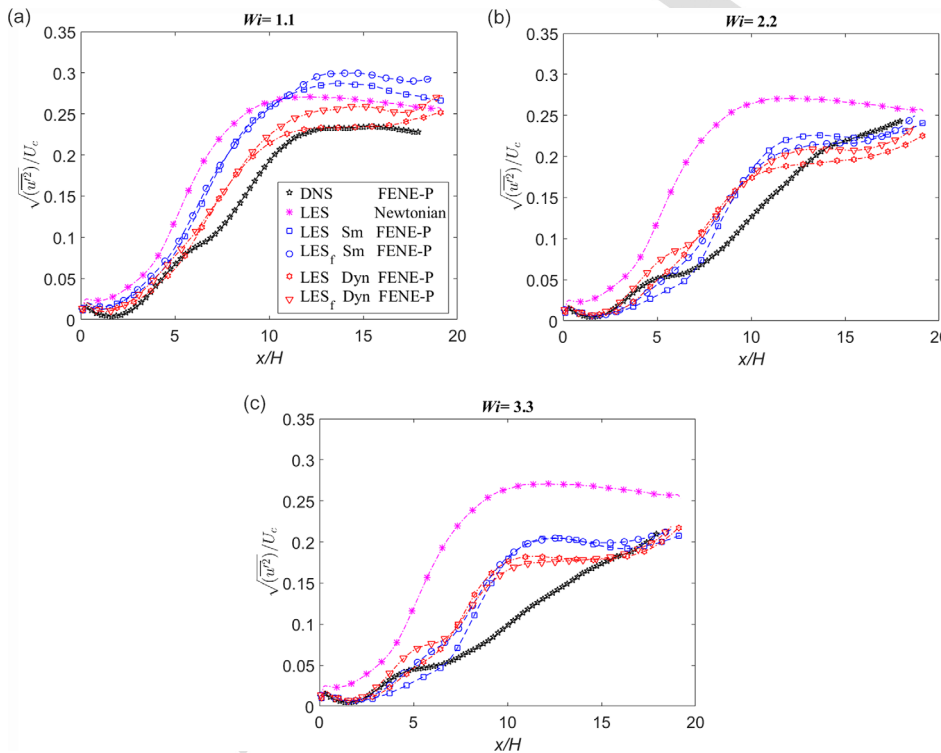


FIG. 17. Effect of SGS stress model on the evolution of the root-mean square of the streamwise velocity fluctuations $\sqrt{u'^2}$ along the centerline, normalized by the centerline mean velocity, for Wi of (a) 1.1, (b) 2.2, and (c) 3.3. The DSIM closure is used for the SGS polymer stretching in the conformation equation and the Smagorinsky (Sm) and dynamic Smagorinsky (Dyn) for the SGS stress in the momentum equation.

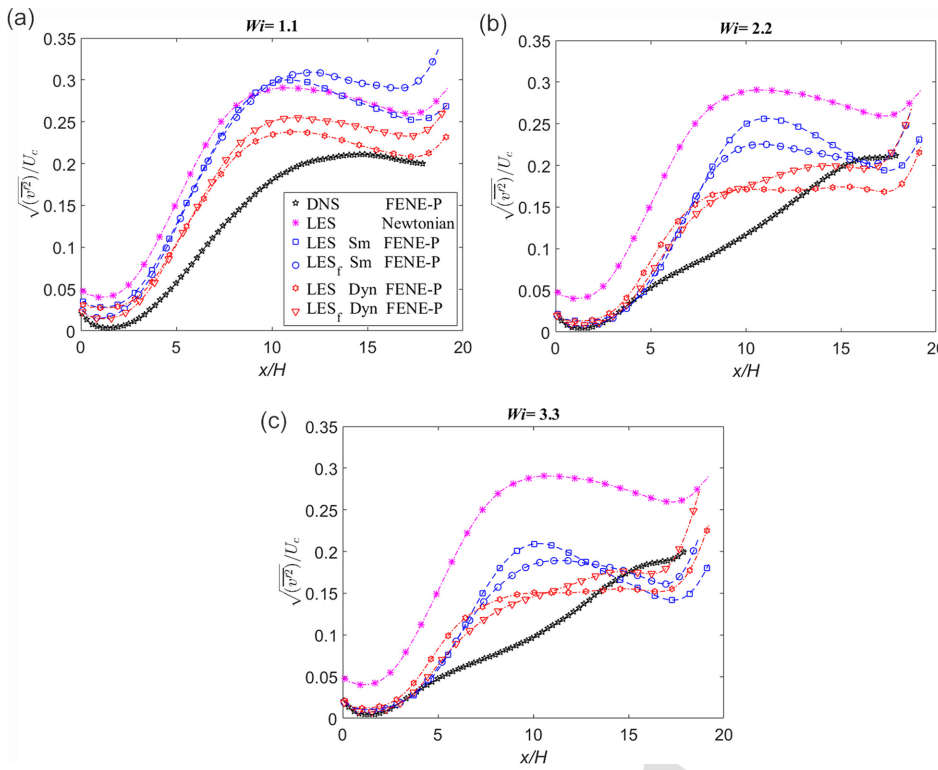


FIG. 18. Effect of SGS stress model on the evolution of the root-mean square of the streamwise velocity fluctuations $\sqrt{v'^2}$ along the centerline, normalized by the centerline mean velocity, for Wi of (a) 1.1, (b) 2.2, and (c) 3.3. The DSIM closure is used for the SGS polymer stretching in the conformation equation and the Smagorinsky (Sm) and dynamic Smagorinsky (Dyn) for the SGS stress in the momentum equation.

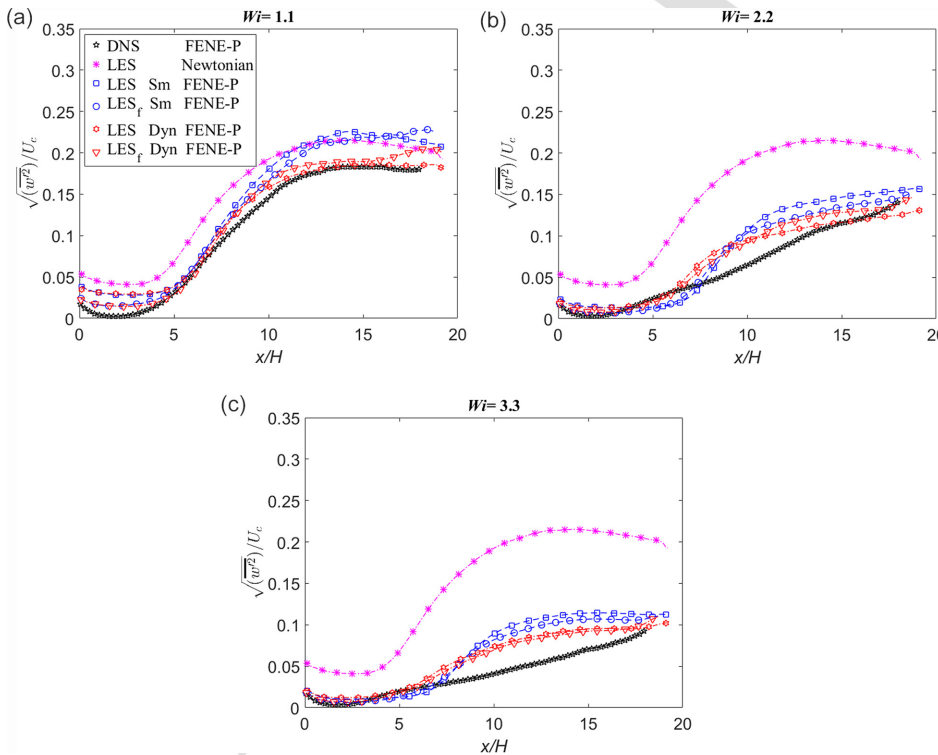


FIG. 19. Effect of SGS stress model on the evolution of the root-mean square of the streamwise velocity fluctuations $\sqrt{w'^2}$ along the centerline, normalized by the centerline mean velocity, for Wi of (a) 1.1, (b) 2.2, and (c) 3.3. The DSIM closure is used for the SGS polymer stretching in the conformation equation and the Smagorinsky (Sm) and dynamic Smagorinsky (Dyn) for the SGS stress in the momentum equation.

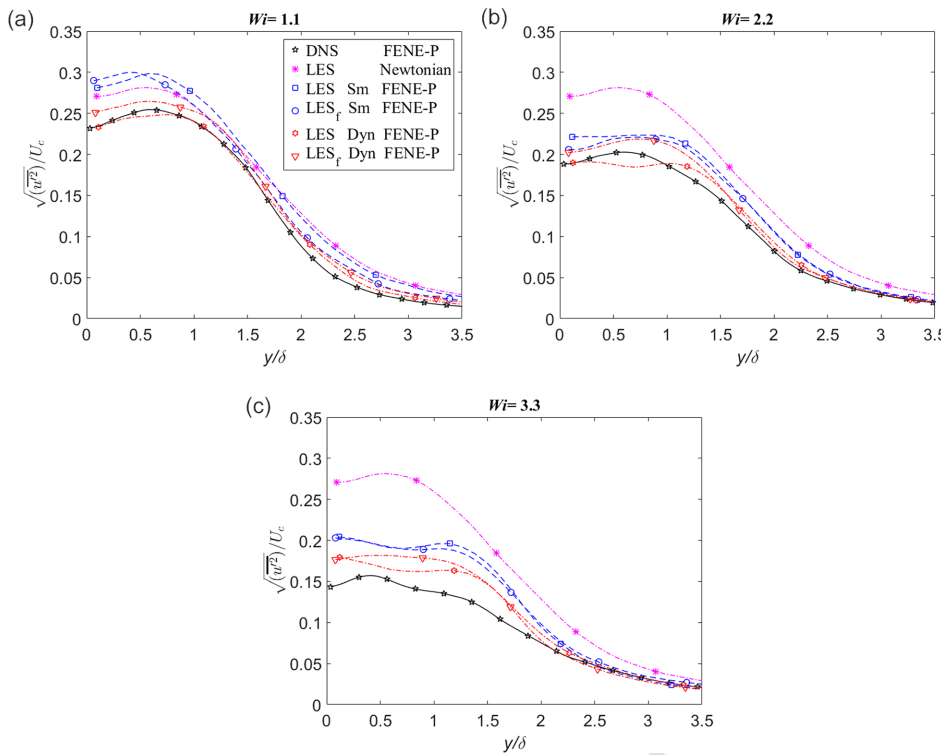


FIG. 20. Effect of SGS stress model on the mean profiles of the rms of the streamwise velocity fluctuations $\sqrt{v'^2}$, normalized by the centerline mean velocity, at $x/H = 12$ for Wi of (a) 1.1, (b) 2.2, and (c) 3.3. The DSIM closure is used for the SGS polymer stretching in the conformation equation and the Smagorinsky (Sm) and dynamic Smagorinsky (Dyn) for the SGS stress in the momentum equation.

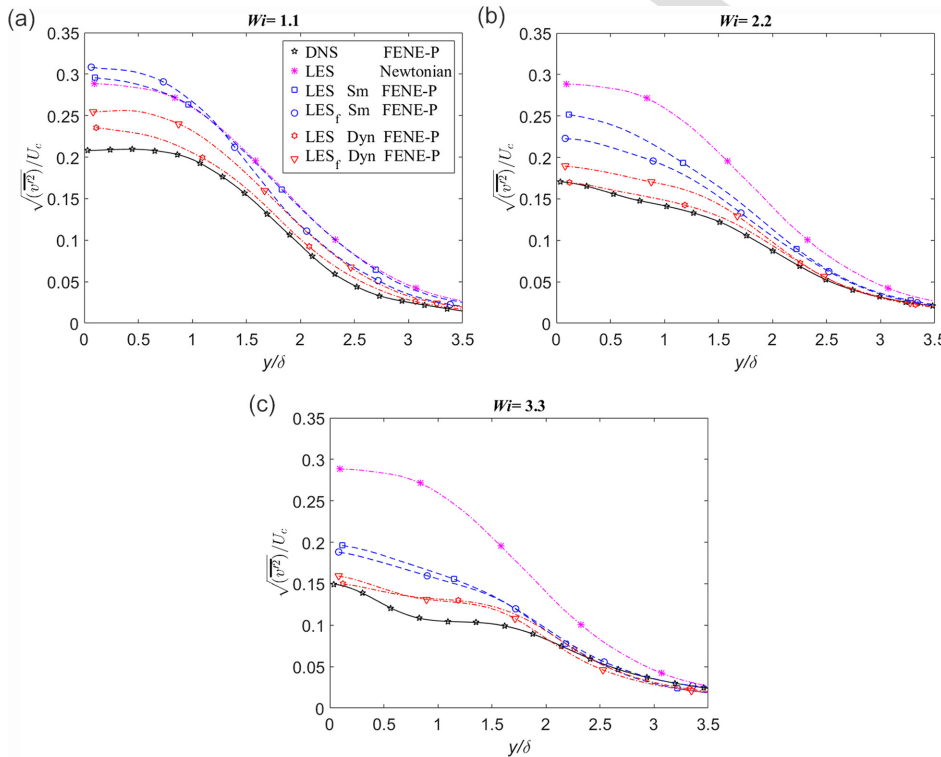


FIG. 21. Effect of SGS stress model on the mean profiles of the rms of the streamwise velocity fluctuations $\sqrt{v'^2}$, normalized by the centerline mean velocity, at $x/H = 12$ for Wi of (a) 1.1, (b) 2.2, and (c) 3.3. The DSIM closure is used for the SGS polymer stretching in the conformation equation and the Smagorinsky (Sm) and dynamic Smagorinsky (Dyn) for the SGS stress in the momentum equation.

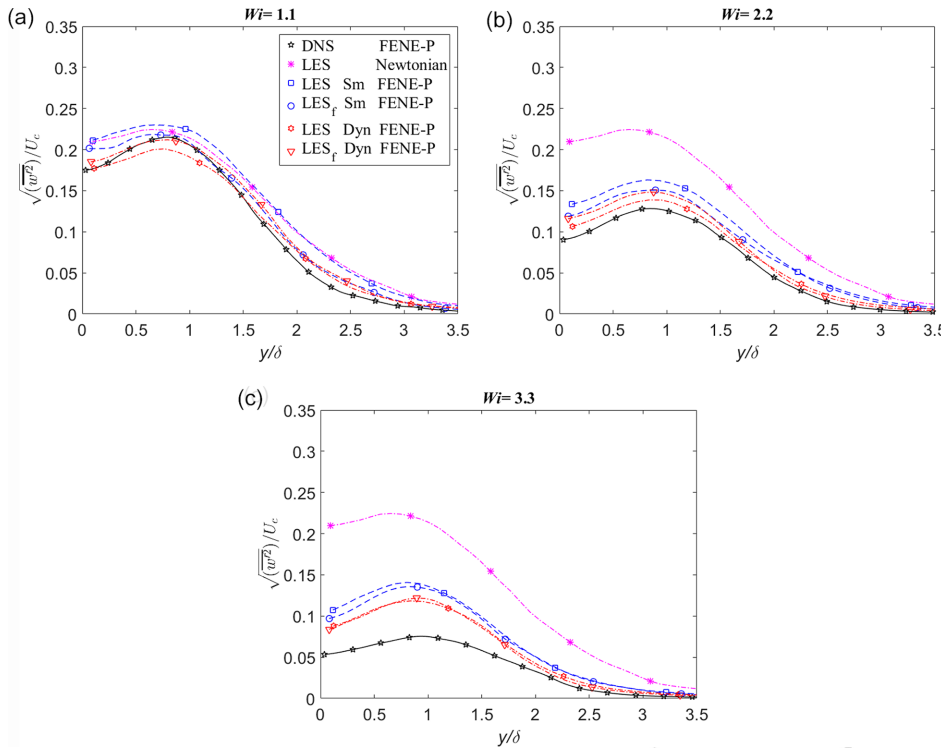


FIG. 22. Effect of SGS stress model on the mean profiles of the rms of the streamwise velocity fluctuations $\sqrt{w'^2}$, normalized by the centerline mean velocity, at $x/H = 12$ for Wi of (a) 1.1, (b) 2.2, and (c) 3.3. The DSIM closure is used for the SGS polymer stretching in the conformation equation and the Smagorinsky (Sm) and dynamic Smagorinsky (Dyn) for the SGS stress in the momentum equation.

$$\varepsilon^s = 2\nu_s \overline{S'_{ij} S'_{ij}}, \quad (43)$$

898 and S'_{ij} is the fluctuating rate-of-strain tensor, obtained from

$$S'_{ij} = \frac{1}{2} \left(\frac{\partial u'_i}{\partial x_j} + \frac{\partial u'_j}{\partial x_i} \right). \quad (44)$$

AQ5 899 As in Sec. VI, the overbar denotes averaging in time and in space in
900 the homogeneous direction.

One of the results obtained by Guimarães *et al.*⁴⁷ in the develop- 901
ment of the theory for viscoelastic planar jets was the identification of 902
the reference velocity and time scales that characterize the flow statis- 903
tics in the self-similar far field region. In particular, they found that the 904
profiles of polymer stress collapse into the same curve when normal- 905
ized by $\tau_{p,ref} = \rho U_c^3(x)r^*(d\delta(x)/dx)/(u^*(x)\delta(x))$. They also showed 906
that for sufficiently high Wi numbers these normalized profiles are 907
universal. 908

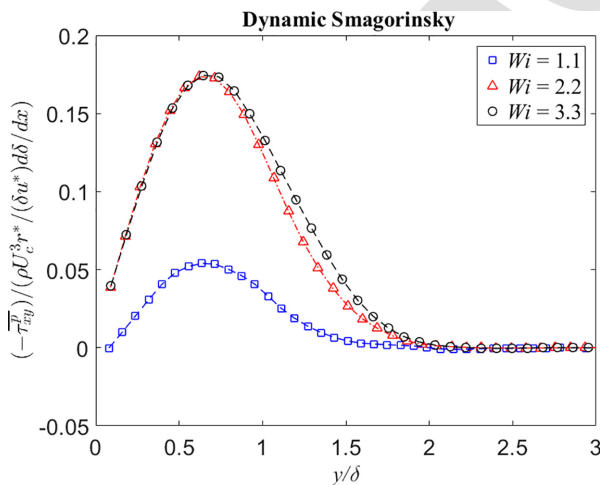


FIG. 23. Mean profiles of polymer shear stresses, normalized as in Guimarães *et al.*,⁴⁷ for several Weissenberg numbers Wi at $x/H = 12$. SGS stress closed by the dynamic Smagorinsky model.

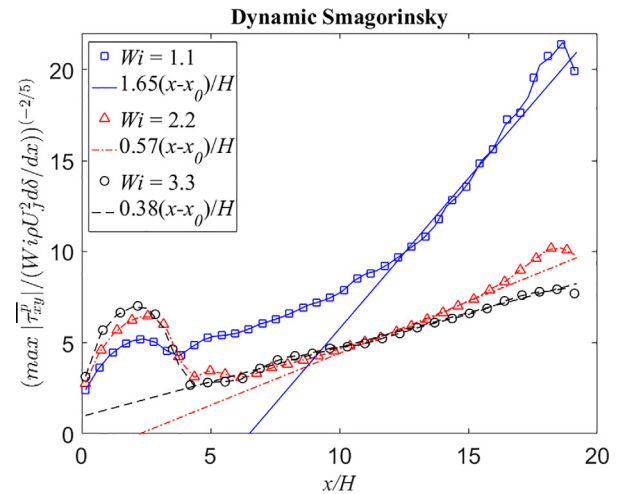


FIG. 24. Streamwise evolution of the maximum value of the mean polymer shear stresses, normalized as in Guimarães *et al.*,⁴⁷ for several Weissenberg numbers. SGS stress closed by the dynamic Smagorinsky model.

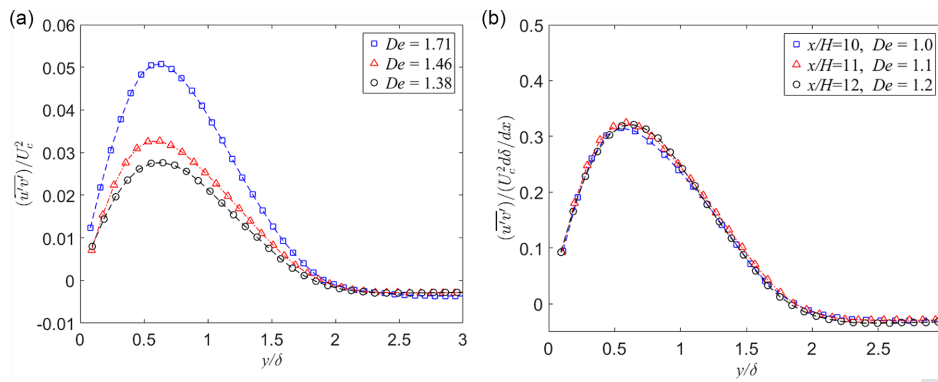


FIG. 25. Transverse profiles of Reynolds shear stresses $\overline{u'v'}$ for several De numbers normalized by (a) U_c^2 all at $x/H = 12$ and by (b) $U_c^2 d\delta(x)/dx$ at $x/H = 10, 11,$ and 12 .

909 Figure 23 shows mean profiles of polymer shear stress normal- 943
 910 ized by $\tau_{p,ref}$ at $x/H = 12$ for several Weissenberg numbers Wi . It is 944
 911 clear that the polymer stresses obtained from the present LES, using 945
 912 the dynamic Smagorinsky and the DSIM closures, collapse at high 946
 913 Weissenberg numbers, in agreement with the theory developed by 947
 914 Guimarães *et al.*⁴⁷ 948
 915 Guimarães *et al.*⁴⁷ also derived the scaling of the decay of the 949
 916 maximum polymer stresses, which is described by the following 950
 917 relation: 951

$$\left(\frac{\tau_c^p(x)}{Wi\rho U_j^2 d\delta(x)/dx} \right)^{-2/5} = A_{\tau_c} \left(\frac{x - x_0}{H} \right), \quad (45)$$

918 where A_{τ_c} is a scaling factor. Figure 24 shows the streamwise evo- 952
 919 lution of the normalized maximum polymer shear stresses 953
 920 obtained by LES, with the SGS stresses given by the dynamic 954
 921 Smagorinsky model. It is clear the present results also display the 955
 922 theoretical $-5/2$ scaling law in the self-similar far-field region, 956
 923 and thus agree with the turbulent viscoelastic jet theory.⁴⁷ 957
 924 Moreover, the constant A_{τ_c} decreases with increasing Wi numbers 958
 925 displaying values that are consistent with the DNS data of 959
 926 Guimarães *et al.*,⁴⁷ particularly for the higher Wi numbers, e.g., 960
 927 $Wi \geq 2$ (compare the values of this factor in Tables I and II). 961
 928 Finally, we assess also the proposed scaling relations for the 962
 929 Reynolds shear stress in viscoelastic turbulent planar jets. 963
 930 Guimarães *et al.*⁴⁷ ascertained that the Reynolds shear stress 964
 931 should be normalized as $\overline{u'v'}/(U_c^2 d\delta(x)/dx)$ for similar values of 965
 932 the Deborah number 966

$$De = \frac{\lambda}{t_c} \quad (46)$$

933 in order to obtain the corresponding self-similar profiles. In Eq. (46), 970
 934 $t_c = \delta(x)/U_c(x)$ is a convective time scale characteristic of the large 971
 935 energy-carrying eddies. 972
 936 Figure 25 shows profiles of normalized Reynolds shear stresses 973
 937 for the present LES at a single location ($x/H = 12$) and $Wi = 1.1, 2.2,$ 974
 938 and 3.3 [Fig. 25(a)], and at different locations $x/H = 10, 11, 12,$ for Wi 975
 939 $= 2.2$ and 3.3 [Fig. 25(b)], but which correspond to approximately the 976
 940 same Deborah numbers ($De \approx 1.0-1.3$). Again, the profiles of the 977
 941 Reynolds stresses normalized as in Guimarães *et al.*⁴⁷ collapse into the 978
 942 same profile [Fig. 25(b)], clearly indicating that the present LES 979
 980
 981

recover the expected theoretical profiles observed in the reference DNS.

VII. CONCLUSIONS

In the present work, the DSIM model developed by Ferreira *et al.*³⁷ for LES of turbulent viscoelastic flows is assessed and tested for the first time in an inhomogeneous turbulent flow configuration. The flow analyzed is a turbulent planar jet, for which a reference DNS exists and a new theory has been recently developed to explain the flow statistics at the far field fully developed turbulent regime (Guimarães *et al.*⁴⁷) The procedure consists in classical *a priori* tests which are based on applying a box filter, with filter sizes $\Delta/\Delta x = 2, 4,$ and 8 to separate the resolved and unresolved/subgrid-scale components of the flow, using the reference DNS of viscoelastic turbulent planar jets carried out by Guimarães *et al.*⁴⁷

The analysis revisited all the assumptions previously used by Ferreira *et al.*³⁷ in isotropic turbulence and considered their validity in turbulent viscoelastic free flows. It turns out that all of these assumptions, and most notably the assumptions of (i) scale similarity of the subgrid-scale polymer stretching terms and (ii) the local equilibrium of the elastic energy production and dissipation, hold remarkably well in the present configuration.

The DSIM model for the SGS polymer stretching term in the constitutive equation, together with the Smagorinsky and dynamic Smagorinsky model for the SGS stress in the momentum equation, was used to carry out LES of the same jets simulated in Guimarães *et al.*⁴⁷ although using much coarser grids. The combined dynamic Smagorinsky model and DSIM model gave the best results and demonstrated the ability to predict the flow structures and the classical one point statistics in the flow with reasonable accuracy.

Future work will focus on the extension of the present model for LES of wall-bounded flows.

ACKNOWLEDGMENTS

The authors acknowledge the financial support of Project Nos. PTDC/EMS-ENE/2390/2014 and POCI-01-0145-FEDER-016669 funded by Fundo Europeu de Desenvolvimento Regional, via COMPETE2020-Programa Operacional Competitividade e Internacionalização (POCI) and Fundação para a Ciência e a Tecnologia. In addition, S.P. and F.T.P. also acknowledge financial

982 support provided by Centro de Estudos de Fenómenos de
983 Transporte through Project Nos. UIDB/00532/2020 and UIDP/
984 00532/2020. C.B.S. is thankful for the support of Fundação para a
985 Ciência e a Tecnologia (FCT), through IDMEC, under LAETA,
986 Project No. UIDB/50022/2020.

987 DATA AVAILABILITY

988 The data that support the findings of this study are available
989 from the corresponding author upon reasonable request.

990 REFERENCES

- 991 ¹B. A. Toms, "Some observations on the flow of linear polymer solutions
992 through straight tubes at large Reynolds numbers," in Proceedings of the 1st
993 International Congress on Rheology, North-Holland, Amsterdam (1949), Vol.
994 2, p. 135.
- 995 ²A. R. Mansour, O. Swaiti, T. Aldoss, and M. Issa, "Drag reduction in turbulent
996 crude oil pipelines using a new chemical solvent," *Int. J. Heat Fluid Flow* **9**, 316
997 (1988).
- 998 ³F. C. Li and Y. Kawaguchi, "Investigation on the characteristics of turbulence
999 transport for momentum and heat in a drag-reducing surfactant solution
1000 flow," *Phys. Fluids* **16**, 3281 (2004).
- 1001 ⁴A. G. Fabula, "Fire-fighting benefits of polymeric drag reduction," *J. Basic Eng.*
1002 *Trans. ASME* **93**(4), 453 (1971).
- 1003 ⁵J. W. Yang, H. Park, H. H. Chun, S. L. Ceccio, M. Perlin, and I. Lee,
1004 "Development and performance at high Reynolds number of a skin-friction
1005 reducing marine paint using polymer additives," *Ocean Eng.* **84**, 183 (2014).
- 1006 ⁶T. J. Ober, D. Foresti, and J. A. Lewis, "Active mixing of complex fluids at the
1007 microscale," *Proc. Natl. Acad. Sci. U. S. A.* **112**(40), 12293 (2015).
- 1008 ⁷J. N. Marhefka and M. V. Kameneva, "Natural drag-reducing polymers:
1009 Discovery, characterization and potential clinical applications," *Fluids* **1**, 6
1010 (2016).
- 1011 ⁸A. Pribush, L. Hatzkelzon, D. Meyerstein, and N. Meyerstein, "The mechanism
1012 of the polymer-induced drag reduction in blood," *Colloids Surf., B* **103**, 354
1013 (2013).
- 1014 ⁹W. J. Orts, R. E. Sojka, and G. M. Glenn, "Polymer additives in irrigation water
1015 to reduce erosion and better manage water infiltration," *Agro-Food-Ind. Hi-*
1016 *Tech* **13**, 37(2002).
- 1017 ¹⁰H. Lee and K. Neville, "The challenge for high polymers in medicine, surgery,
1018 and artificial internal organs," *J. Macromol. Sci.* **4**(3), 757 (1970).
- 1019 ¹¹P. C. Sousa, F. T. Pinho, M. S. N. Oliveira, and M. A. Alves, "Extensional flow
1020 of blood analog solutions in microfluidic devices," *Biomicrofluidics* **5**(1),
1021 014108 (2011).
- 1022 ¹²J. L. Lumley, "Drag reduction by additives," *Annu. Rev. Fluid Mech.* **1**, 367
1023 (1969).
- 1024 ¹³P. S. Virk, "Drag reduction fundamentals," *AIChE J.* **21**(4), 625 (1975).
- 1025 ¹⁴C. M. White and M. G. Mungal, "Mechanics and prediction of turbulent drag
1026 reduction with polymer additives," *Annu. Rev. Fluid Mech.* **40**, 235 (2008).
- 1027 ¹⁵S. B. Pope, *Turbulent Flows* (Cambridge University Press, Cambridge, 2000).
- 1028 ¹⁶P. Sagaut, *Large Eddy Simulation for Incompressible Flows*, 3rd ed. (Springer,
1029 Berlin, 2005).
- 1030 ¹⁷J. Jiménez, "Computing high-Reynolds-number turbulence: Will simulations
1031 ever replace experiments?," *J. Turbul.* **4**, N22 (2003).
- 1032 ¹⁸O. Reynolds, "On the dynamical theory of incompressible viscous fluids and
1033 the determination of the criterion," *Philos. Trans. R. Soc. London, Ser. A* **186**,
1034 123 (1895).
- 1035 ¹⁹F. T. Pinho, C. F. Li, B. A. Younis, and R. Sureshkumar, "A low Reynolds num-
1036 ber turbulence closure for viscoelastic fluids," *J. Non-Newtonian Fluid Mech.*
1037 **154**, 89 (2008).
- 1038 ²⁰F. T. Pinho, C. F. Li, B. A. Younis, and R. Sureshkumar, "Corrigendum to "A
1039 low Reynolds number turbulence closure for viscoelastic fluids,"" *J. Non-*
1040 *Newtonian Fluid Mech.* **51**, 181 (2012).
- 1041 ²¹P. R. Resende, K. Kim, B. A. Younis, R. Sureshkumar, and F. T. Pinho, "A
1042 FENE-P $k-\epsilon$ turbulence model for low and intermediate regimes of polymer-
1043 induced drag reduction" *J. Non-Newtonian Fluid Mech.* **166**, 639 (2011).
- ²²G. Iaccarino, E. S. G. Shaqfeh, and Y. Dubief, "Reynolds-averaged modeling of
1044 polymer drag reduction in turbulent flows," *J. Non-Newtonian Fluid Mech.*
1045 **165**, 376 (2010).
- ²³M. Masoudian, K. Kim, F. T. Pinho, and R. Sureshkumar, "A viscoelastic $k-\epsilon$ -
1046 v^2-f turbulent flow model valid up to the maximum drag reduction limit,"
1047 *J. Non-Newtonian Fluid Mech.* **202**, 99 (2013).
- ²⁴J. Smagorinsky, "General circulation experiments with the primitive equa-
1050 tions," *Mon. Weather Rev.* **91**(3), 99 (1963).
- ²⁵J. Deardorff, "A numerical study of three-dimensional turbulent channel flow
1052 at large Reynolds numbers," *J. Fluid Mech.* **41**(2), 453 (1970).
- ²⁶M. Lesieur and O. Metais, "New trends in large eddy simulations of
1054 turbulence," *Annu. Rev. Fluid Mech.* **28**, 45 (1996).
- ²⁷U. Piomelli, "Large-eddy simulation: Achievements and challenges," *Prog.*
1056 *Aerosp. Sci.* **35**, 335 (1999).
- ²⁸C. Meneveau and J. Katz, "Scale-invariance and turbulence models for large
1058 eddy simulation," *Annu. Rev. Fluid Mech.* **32**, 1 (2000).
- ²⁹C. B. Silva and O. Metais, "On the influence of coherent structures upon inter-
1060 scale interactions in turbulent plane jets," *J. Fluid Mech.* **473**, 103 (2002).
- ³⁰R. B. Bird, R. C. Armstrong, and O. Hassager, *Dynamics of Polymeric Liquids*,
1062 *Volume 1: Fluid Mechanics* (John Wiley Press, New York, 1987).
- ³¹R. B. Bird, C. F. Curtiss, R. C. Armstrong, and O. Hassager, *Dynamics of*
1064 *Polymeric Liquids, Volume 2: Kinetic Theory* (John Wiley Press, New York,
1065 1987).
- ³²Q. Zhou and R. Akhavan, "A comparison of FENE and FENE-P dumbbell and
1067 chain models in turbulent flow," *J. Non-Newtonian Fluid Mech.* **109**, 115
1068 (2003).
- ³³M. Herrchen and H. C. Ottinger, "A detailed comparison of various FENE
1070 dumbbell models," *J. Non-Newtonian Fluid Mech.* **68**, 17 (1997).
- ³⁴R. B. Bird, P. J. Dotson, and N. L. Johnson, "Polymer solution rheology based
1072 on a finitely extensible bead-spring chain model," *J. Non-Newtonian Fluid*
1073 *Mech.* **7**, 213 (1980).
- ³⁵A. Peterlin, "Streaming birefringence of soft linear macromolecules with finite
1075 chain length," *Polymer* **2**, 257 (1961).
- ³⁶Y. Dubief, V. Terrapon, and J. Soria, "On the mechanism of elasto-inertial
1077 turbulence," *Phys. Fluids* **25**, 110817 (2013).
- ³⁷P. O. Ferreira, F. T. Pinho, and C. B. Silva, "Large-eddy simulations of forced
1079 isotropic turbulence with viscoelastic fluids described by the FENE-P model,"
1080 *Phys. Fluids* **28**, 125104 (2016).
- ³⁸H. D. Xi, E. Bodenschatz, and H. Xu, "Elastic energy flux by flexible polymers
1082 in fluid turbulence," *Phys. Rev. Lett.* **111**, 24501 (2013).
- ³⁹P. C. Valente, C. B. Silva, and F. T. Pinho, "The effect of viscoelasticity on the
1084 turbulent kinetic energy cascade," *J. Fluid Mech.* **760**, 39 (2014).
- ⁴⁰P. C. Valente, C. B. Silva, and F. T. Pinho, "Energy spectra in inertio-elastic
1086 turbulence," *Phys. Fluids* **28**, 075108 (2016).
- ⁴¹T. Watanabe and T. Gotoh, "Hybrid Eulerian-Lagrangian simulations for
1088 polymer-turbulence interactions," *J. Fluid Mech.* **717**, 535 (2013).
- ⁴²T. Ohta and M. Miyashita, "DNS and LES with an extended Smagorinsky
1090 model for wall turbulence in non-Newtonian viscous fluids," *J. Non-*
1091 *Newtonian Fluid Mech.* **206**, 29 (2014).
- ⁴³L. Thais, A. E. Tejada-Martinez, T. B. Gatski, and G. Mompean, "Temporal
1093 large eddy simulations of turbulent viscoelastic drag reduction flow," *Phys.*
1094 *Fluids* **22**, 13103 (2010).
- ⁴⁴L. Wang, W. H. Cai, and F. C. Li, "Large-eddy simulations of a forced homoge-
1096 nous isotropic turbulence with polymer additives," *China Phys. B* **23**, 34701
1097 (2014).
- ⁴⁵J. Li, B. Yu, S. Sun, D. Sun, and Y. Kawaguchi, "An N-parallel FENE-P consti-
1099 tutive model and its application in large-eddy simulation of viscoelastic turbu-
1100 lent drag-reducing flow," *J. Comput. Sci.* **29**, 70 (2018).
- ⁴⁶M. Masoudian, C. B. Silva, and F. T. Pinho, "Grid and sub-grid scale interac-
1102 tions in viscoelastic turbulent flow and implications for modelling," *J. Turbul.*
1103 **17**(6), 543 (2016).
- ⁴⁷M. C. Guimarães, N. Pimentel, F. T. Pinho, and C. B. da Silva, "Direct
1105 numerical simulations of turbulent viscoelastic jets," *J. Fluid Mech.* **899**, A11-1
1106 (2020).
- ⁴⁸D. Lopes, "Direct and large-eddy simulations of the turbulent entrainment of
1108 passive scalars in planar jets," Ph.D. thesis (Instituto Superior Técnico, 2014).
1109

AQ6

- 1110 ⁴⁹C. B. Silva, D. C. Lopes, and V. Raman, "The effect of subgrid-scale models on the
1111 entrainment of a passive scalar in a turbulent planar jet," *J. Turbul.* **16**(4),
1112 342 (2015).
- 1113 ⁵⁰J. Smagorinsky, "General circulation experiments with the primitive equations:
1114 I. The basic experiment," *Mon. Weather Rev.* **91**(3), 99 (1963).
- 1115 ⁵¹M. Germano, U. Piomelli, P. Moin, and W. H. Cabot, "A dynamic subgrid-
1116 scale eddy viscosity model," *Phys. Fluids A* **3**, 1760 (1991).
- 1117 ⁵²R. Reis, "The dynamics of coherent vortices near the turbulent/non-turbulent
1118 interface analysed by direct numerical simulations," Ph.D. thesis (Instituto
1119 Superior Técnico, 2011).
- 1120 ⁵³S. K. Lele, "Compact finite difference schemes with spectral-like resolution,"
1121 *J. Comp. Phys.* **103**, 15 (1992).
- 1122 ⁵⁴S. A. Orszag, "Numerical methods for the simulation of turbulence," *Phys.*
1123 *Fluids*. **12**(12), II-250 (1969).
- 1124 ⁵⁵F. Dupret and J. M. Marchal, "Loss of evolution in the flow of viscoelastic flu-
1125 ids," *J. Non-Newtonian Fluid Mech.* **20**, 143-171 (1986).
- 1126 ⁵⁶R. Sureshkumar and A. N. Beris, "Effect of artificial stress diffusivity on the sta-
1127 bility of numerical calculations and the flow dynamics of time-dependent vis-
1128 coelastic flows," *J. Non-Newtonian Fluid Mech.* **60**, 53 (1995).
- 1129 ⁵⁷T. Min, J. Y. Yoo, and H. Choi, "Effect of spatial discretization schemes on
1130 numerical solutions of viscoelastic fluid flows," *J. Non-Newtonian Fluid Mech.*
1131 **100**, 27 (2001).
- 1132 ⁵⁸Y. Dubief and S. K. Lele, *Direct Numerical Simulation of Polymer Flow* (Center
1133 for Turbulence Research, Annual Research Briefs, NASA, AMES/Stanford
1134 University, 2001), p. 197.
- 1135 ⁵⁹B. Yu and Y. Kawaguchi, "Direct numerical simulation of viscoelastic drag-
1136 reducing flow: A faithful finite difference method," *J. Non-Newtonian Fluid*
1137 *Mech.* **116**, 431 (2004).
- 1138 ⁶⁰T. Vaithianathan and L. R. Collins, "Numerical approach to simulating turbu-
1139 lent flow of a viscoelastic polymer solution," *J. Comput. Phys.* **187**(1), 1 (2003).
- 1140 ⁶¹T. Vaithianathan, A. Robert, J. G. Brasseur, and L. R. Collins, "An improved
1141 algorithm for simulating three-dimensional, viscoelastic turbulence," *J. Non-*
1142 *Newtonian Fluid Mech.* **140**(3), 3 (2006).
- 1143 ⁶²A. Kurganov and E. Tadmor, "New high-resolution central schemes for nonlin-
1144 ear conservation laws and convection-diffusion equations," *J. Comput. Phys.*
1145 **160**, 241 (2000).
- 1146 ⁶³W. Cai, F. Li, and H. Zhang, "DNS study of decaying homogeneous isotropic
1147 turbulence with polymer additives," *J. Fluid Mech.* **665**, 334 (2010).
- 1148 ⁶⁴S. Parvar, C. B. da Silva, and F. T. Pinho, "Local similarity solution for steady
1149 laminar planar jet flow of viscoelastic FENE-P fluids," *J. Non-Newtonian Fluid*
1150 *Mech.* **279**, 104265 (2020).
- 1151 ⁶⁵S. Parvar, C. B. da Silva, and F. T. Pinho, "Corrigendum to "Local similarity
1152 solution for steady laminar planar jet flow of viscoelastic FENE-P fluids,""
1153 *J. Non-Newtonian Fluid Mech.* **279**, 104265 (2020); **281**, 104309 (2020).
- 1154 ⁶⁶S. Liu, C. Meneveau, and J. Katz, "On the properties of similarity subgrid-scale
1155 models as deduced from measurements in a turbulent jet," *J. Fluid Mech.* **275**, 83 (1994).
- 1156 ⁶⁷J. Bardina, J. H. Ferziger, and W. C. Reynolds, Improved subgrid model for
1157 large-eddy simulation," AIAA Paper No. 80-1357 (1980).
- 1158 ⁶⁸A. W. Vreman, "An eddy-viscosity subgrid-scale model for the turbulent shear
1159 flow: Algebraic theory and applications," *Phys. Fluids* **16**(10), 3670 (2004).
- ⁶⁹E. Léveque, F. Toschi, L. Shao, and J.-P. Bertoglio, "Shear-improved
Smagorinsky model for large-eddy simulation of wall bounded turbulent
flows," *J. Fluid Mech.* **570**, 491-502 (2007).
- ⁷⁰R. Sureshkumar, A. N. Beris, and R. A. Handler, "Direct numerical simulation
of the turbulent channel flow of a polymer solution," *Phys. Fluids* **9**, 743
(1997).
- ⁷¹K. Kim, C. Li, R. Sureshkumar, S. Balachandar, and R. J. Adrian, "Effects of
polymer stresses on eddy structures in drag-reduced turbulent channel flow,"
J. Fluid Mech. **584**, 281 (2007).
- ⁷²K. Horiuti, K. Matsumoto, and K. Fujiwara, "Remarkable drag reduction in
non-affine viscoelastic turbulent flows," *Phys. Fluids* **25**, 015106 (2013).
- ⁷³M. D. Graham, "Drag reduction and the dynamics of turbulence in simple and
complex fluids," *Phys. Fluids* **26**(10), 101301 (2014).
- ⁷⁴G. E. Gadd, "Turbulence damping and drag reduction produced by certain
additives in water," *Nature* **206**(4983), 463-467 (1965).
- ⁷⁵G. E. Gadd, "Reduction of turbulent friction in liquids by dissolved additives,"
Nature **212**(5065), 874-877 (1966).
- ⁷⁶A. White, in *Some Observations on the Flow Characteristics of Certain Dilute*
Macromolecular Solutions, Viscous Drag Reduction, edited by C. S. Wells
(Springer, 1969), pp. 297-311.
- ⁷⁷A. White, "Turbulence and drag reduction with polymer additives," Ph.D. the-
sis (Middlesex Polytechnic, 1972).
- ⁷⁸J. Wu, "Drag reduction in external flows of additive solutions," in *Viscous Drag*
Reduction, edited by C. S. Wells (Springer, 1969), pp. 331-350.
- ⁷⁹E. Gutmark and I. Wygnansky, "The planar turbulent jet," *J. Fluid Mech.* **73**,
465 (1976).
- ⁸⁰L. J. S. Browne, R. A. Antonia, S. Rajagopalan, and A. J. Chambers,
"Interaction region of a two-dimensional turbulent plane jet in still air," in
Structure of Complex Turbulent Shear Flow, IUTAM Symposium, edited by R.
Dumas and L. Fulachier (Springer, Marseille, 1982).
- ⁸¹F. O. Thomas and H. C. Chu, "An experimental investigation of the transition
of the planar jet: Subharmonic suppression and upstream feedback," *Phys.*
Fluids **1**(9), 1566 (1989).
- ⁸²R. C. Deo, J. Mi, and G. J. Nathan, "The influence of Reynolds number on a
plane jet," *Phys. Fluids* **20**(7), 075108 (2008).
- ⁸³R. C. Deo, G. J. Nathan, and J. Mi, "Similarity analysis of the momentum field
of a subsonic, plane air jet with varying jet-exit and local Reynolds numbers,"
Phys. Fluids **25**, 015115 (2013).
- ⁸⁴S. Stanley, A. Sarkar, and J. P. Mellado, "A study of the flowfield evolution and
mixing in a planar turbulent jet using direct numerical simulation," *J. Fluid*
Mech. **450**, 377 (2002).
- ⁸⁵N. S. Berman and H. Tan, "Two-component laser doppler velocimeter stud-
ies of submerged jets of dilute polymer solutions," *AIChE J.* **31**(2), 208
(1985).
- ⁸⁶K. Koziol and P. Glowacki, "Turbulent jets of dilute polymer solutions,"
J. Non-Newtonian Fluid Mech. **32**(3), 311 (1989).
- ⁸⁷A. A. Townsend, *The Structure of Turbulent Shear Flow* (Cambridge University
Press, Cambridge, 1976).
- ⁸⁸J. L. Lumley, "Drag reduction in turbulent flow by polymer additives,"
J. Polym. Sci. **7**(1), 263 (1973).